A DEVELOPMENT OF A DYNAMIC ANALYSIS TECHNIQUE FOR VEHICLE FRAMES OF VIBRATORY PLOWS AND TRENCHERS

By

DAVID LYNN TURNEY

Bachelor of Science
Louisiana Tech University
Ruston, Louisiana
1973

Master of Science
Oklahoma State University
Stillwater, Oklahoma
1975

Submitted to the Faculty of the Graduate College
of the Oklahoma State University
in partial fulfillment of the requirements
for the Degree of
DOCTOR OF PHILOSOPHY
July, 1978

A DEVELOPMENT OF A DYNAMIC ANALYSIS TECHNIQUE

FOR VEHICLE FRAMES OF VIBRATORY

PLOWS AND TRENCHERS

Thesis Approved:

Donald E. Boyd
Thesis Adviser

R L Lowery

Allen E. Kelly

Ladislaus J. Fila

Norman N Durham
Dean of the Graduate College

ACKNOWLEDGMENTS

The aid of those who helped during this study is gratefully acknowledged. I would like to express my appreciation to Dr. Donald E. Boyd, my major adviser, for his advice, instruction, and encouragement during my graduate study. My thanks are extended to Drs. A. E. Kelly, R. L. Lowery, and L. J. Fila for serving on my committee.

I would like to acknowledge Dr. Gerald Stangl of Charles Machine Works for his cooperation and assistance in providing data and machine behavior.

My appreciation is expressed also to Twila Longan, Charlene Fries, and Eldon Hardy for their assistance in preparing the final manuscript.

I owe a special word of gratitude to my wife, Donna, and son, Lewis, for their sacrifice, patience, understanding, and encouragement during my graduate study. I also wish to thank my parents who have continually encouraged me throughout my educational endeavors.

The School of Mechanical and Aerospace Engineering provided a Graduate Assistantship which helped make my graduate study possible.

TABLE OF CONTENTS

LIST OF TABLES

LIST OF FIGURES

LIST OF SYMBOLS

a	distance from the point of rotation to plow c.g. for the simple model
a_i, b_i, d_i	X, Y, and Z components of the position vector of a point with respect to the body c.g.
AM_i	acceleration vector for a concentrated mass
bp_{201}	horizontal distance from front axle pin to tire contact point
[C]	damping matrix
C_i	damping coefficient
CB	ratio of output over input angle for plow linkage
CCH	damping coefficient for digging chain teeth
CCI_i	inertia value at the added mass point
CCM_i	added mass value for the 2-D model
d	distance from the point of rotation to the ground stiffness for the simple model
dp_{200}	vertical distance from front axle pin to axle c.g.
dp_{201}	vertical distance from front axle pin to tire contact point
e_i, f_i, g_i	X, Y, and Z components of the position vector of a point with respect to a known reference
F_A	rotating shaker force vector
{FC}	reference input velocity load matrix
FD_i	total force in the damping element
{FK}	reference input displacement load matrix
FLF	length of uniform frame in front of the front axle
FLR	length of uniform frame behind the front axle

FLT	total length of uniform frame section
FS_i	total force in the spring element
FTG	static force on one tooth of the digging chain
FTH	total force on the digging chain tooth
$F\lambda_i$	frame forces in X, Y, and Z directions, respectively
h_z	vertical distance from frame c.g. to cab c.g.
I_i	inertia value of the body (2-D)
$[I_i]$	inertia matrix of the body (3-D)
IXX_i	coefficients of the inertia matrix
[K]	stiffness matrix
K_i	stiffness coefficient
KE	kinetic energy
L	Lagrangian
ℓ_i	length of the plow assembly links
ℓ, m, n	set of unit vectors parallel to X, Y, and Z axes
ℓh_i	perpendicular distance from link ℓ_2 to a point on the plow blade
ℓv_i	distance along link ℓ_2 from the upper plow arm connecting pin to a point on the plow blade
[M]	mass matrix
M_i	mass of the body
PE	potential energy
Q	generalized forces
q	generalized coordinates
{R}	total load matrix
RCH	total digging chain force
RD	Rayleigh's dissipation function
REC	reduction factor for ground damping

RED	reduction factor for digging tooth damping
REH	reduction factor for digging tooth static force
REK	reduction factor for ground stiffness
RPF	resultant plow force vector
$SRMY_i$	bending stress resultant in the frame
SRX_i	axial stress resultant in the frame
SRZ_i	shear stress resultant in the frame
TS	tooth spacing for the digging chain
$T\lambda_i$	moments applied to the frame in the X, Y, and Z directions, respectively
U, V, W	fixed axis system for the cab
u, v, w	displacements in the U, V, and W directions, respectively
V_i	velocity vector for a point
VC_i	velocity in a damping element due to the generalized coordinates
VCH	digging chain velocity
VM_i	velocity vector for a body center of mass
VR_i	input reference velocity
VS	forward velocity of the vehicle parallel to the ground
$V\lambda_i$	components of the velocity vector for a point
$VM\lambda_i$	components of the velocity vector for a body center of mass
WE	external work
X, Y, Z	fixed axis system for the frame assembly
x, y, z	displacements in the X, Y, and Z directions, respectively
XIC_i, ZIC_i	coordinates of the attachment point for the added masses
XIM_i, ZIM_i	coordinates of the added masses with respect to a known reference
XK_i	displacement of a spring element due to the generalized coordinates

XM_i, ZM_i	coordinates of the added masses with respect to the frame c.g.
XOP_i, ZOP_i	coordinates of the frame output points
XP_i, ZP_i	coordinates of a plow blade point in the axis system ℓ^*-n^*
XR_i	input reference displacement
ρ	mass density/unit length of uniform frame
ρ_i	position vector of a point
Δ_i	displacement vector of a point
$\Delta\lambda_i$	components of the displacement vector
ω_i	rotational vector for a body
$\omega\lambda_i$	components of the rotational vector
ω_η	natural frequency of front axle
ω_ψ	natural frequency for the ψ coordinate of the plow assembly
ω_α	natural frequency for the α coordinate of the plow assembly
θ_g	angle between the ground and the X-axis (2-D)
θ_{ch}	angle between the digging chain boom and the X-axis
θ_x, θ_y, θ_z	rotations about X, Y, and Z, respectively
θ_u, θ_v, θ_w	rotations about U, V, and W, respectively
ψ	rotation of the upper plow arm
ψ_1	rotation of link ℓ_2 due to ψ
ψ_3	angle of the lift cylinder
ψ_6	total rotation of link ℓ_2
α	rotation of the plow boom
η	rotation of the front axle
β	plow blade steer angle
δ_F	front wheel steering angle
δ_R	rear wheel steering angle

ϕ	angle of the resultant plow force
λCG_i	location of the body c.g. with respect to a known reference

Subscripts

1	frame assembly
2	plow assembly
3	cab
4	front axle
i	refers to numbered points and elements on the model
j	refers to the generalized coordinates

Notes

(1)	a dot above a quantity denotes time derivative
(2)	a prime superscript denotes the initial position of an angle
(3)	a superscript T indicates the transpose of a matrix
(4)	a double prime, triple prime, and asterisk all denote a rotated axis system
(5)	a bar over a quantity indicates a modified value due to a change in c.g. location
(6)	a λ indicates X, Y, Z (i.e., $F\lambda_i$ implies FX_i, FY_i, FZ_i)

CHAPTER I

INTRODUCTION

As the demands of industry require more functional, efficient, and safe equipment, the role of dynamic analysis in the design process becomes more important. Problems such as riding comfort, handling stability, impact loading, and frame and body fatigue life are all related to dynamic problems and cannot be adequately solved with only a static analysis. The need for further development of dynamic design and analysis tools in the earthmoving, construction, and agricultural industries is greater today than ever before. The purpose of this research is to develop a dynamic analysis technique which can be quickly and efficiently applied to the design of basic frame-type equipment considering the effects of ground profile and external attachments.

Background

The complete development program includes both analytical methods and testing. Conceptually, field testing is the best answer for final design and evaluation of a product. However, it is not suitable in the initial and intermediate design stages because of the following reasons.

1. It comes after the machine is built.
2. It may be impossible to test cases which can be studied analytically.
3. Fatigue life problems may take months or years to test adequately.

Analytical methods allow the designer more flexibility than does testing. The importance of mathematical simulation in the design process was vividly expressed by Miers (1). Mathematical modeling and simulation techniques can effectively support design and testing programs and provide the key to shrinking development time and money.

Static analysis and testing have been the primary tools for the design of industrial and agricultural equipment. For example, vibratory plows were investigated by Boyd and Turney (2) (3) in which an analytical static analysis procedure for the frame was developed. The total machine was modeled and the results were verified with a limited amount of field test data. A complete laboratory and field test program for both static and dynamic stresses in a tractor shovel was described by Hayden (4).

The automotive industry is performing dynamic analysis with finite element methods incorporated into a systems approach. Horvath (5) described the typical analysis procedure used at this time by Cadillac Motor Division. The vehicle is substructured, a modal analysis performed for each part, and the total system added together for the complete response. Computer programs such as NASTRAN are used for the analysis. Reference (6) contains the evaluation of an automotive frame model for dynamic analysis developed by the Ford Motor Company.

Techniques for dynamic analysis in earthmoving equipment were presented in Reference (7). This work was also based upon the systems approach with finite element modeling. Fanslow (8) briefly described the design procedure and analysis techniques used by International Harvester Company to develop a 200 hp tractor. The work included a finite element frame model.

A different approach for the dynamic frame analysis of agricultural equipment was taken by Smith (9). He formulated the overall vehicle model considering the frame rigid and generated the time dependent suspension forces. These loads were then applied to a finite element frame model and the dynamic stresses calculated.

Much work has been done in the area of rigid body dynamics concerning tractor motion. However, most of the research has been aimed at riding qualities, handling characteristics, and stability. Pershing and Yoerger (10) formulated a linear three-dimensional model for a tractor and studied the transient motion of hitting a bump while operating on a side slope. A computer simulation was made by Smith (11) whose model included the chassis, cab, and seat. Nonlinear representation was used for the tires and cab mounts. The model had 13 degrees of freedom and small displacements were assumed.

Tractor models have also been used which considered nonlinear three-dimensional motion. Reference (12) describes a model of this type which included the tractor chassis as one rigid body having six degrees of freedom and a pin-connected front axle having one additional degree of freedom. Therefore, a total of seven degrees of freedom was used for the entire system. Computer programs for simulating the motion of both two- and four-wheel drive tractors along with computer graphics output were briefly described in Reference (13).

No research which attempts to include the effects of external implements (e.g., plows and trenchers) in the frame design of agricultural equipment was found in the literature survey. Reference (14) contains the model of a planter but the towing tractor was not included. The response was obtained by applying forces at the implement connecting points.

The mechanics of the forces applied through the various implements must be understood before they can be adequately modeled. A limited amount of information derived from both testing and the application of soil mechanics of vibratory plows can be found in the literature concerning this (15) through (19).

Smith's (9) frame analysis combined the rigid body motion studies with the finite element method. This technique is very useful when the primary concern is frame design. However, Smith's model had only three rigid body motions and did not include attachments. Therefore, a need still exists for further development of a more general dynamic analysis procedure which can improve the frame design of various frame-type equipment.

Approach to the Problem

The first objective of this study was to develop an overall model of the vehicle including the vibratory plow and digging chain. Two formulations were made: one for two-dimensional (2-D) motion and one for three-dimensional (3-D) motion. For both cases the tires and cab mounts were considered to be combinations of linear springs and damping elements. The ground coefficients were allowed to be discretely discontinuous and depended on the rigid body displacements. Therefore, the plow, digging boom, and digging chain forces were also discontinuous.

The forcing function for the vibratory plow was observed to be the rotating shaker force. The force was periodic and acted in the plane of the plow blade. The digging chain forcing function was random, discontinuous, and both time- and displacement-dependent. Reference

displacements and velocities were allowed as functions of time at all tires to simulate ground effects.

The equations of motion were written for both cases using the Lagrangian approach. These equations were numerically integrated using a Runge-Kutta fourth-order technique. The tire, plow, and cab mount forces were evaluated for the rigid body motion. The internal components (i.e., reel, reel carrier, engine, etc.) were then considered separately and the frame attachment forces calculated. The derivations of the equations for the 2-D case and the 3-D case are given in Chapters II and III, respectively.

Separate computer programs were written for the 2-D and 3-D cases. Chapter IV contains a brief description of each program along with a table showing the basic sequence of operations.

Several studies are presented herein to illustrate some of the capabilities of the analysis programs and to evaluate the results qualitatively. The stresses generated for this thesis are attributed to dynamic loading only. Thus, the total frame stresses can be obtained by superposition of the static and dynamic analysis. The static stresses can be calculated by programs STRAIGHT (2) and OFFSET (3) for the 2-D model and the 3-D model, respectively. The verification of the programs and the results of the studies made are presented in Chapter V. Chapter VI contains the summary, conclusions, and recommendations of this research.

CHAPTER II

DEVELOPMENT OF THE TWO-DIMENSIONAL CASE

Lagrangian Formulation

The equations of motion for the 2-D case were derived using the model shown in Figures 1 through 3. The masses of the frame, plow, and cab assemblies were denoted as M_1, M_2, and M_3, respectively. Correspondingly, the inertia value for each body about its center of gravity (c.g.) was defined as I_1, I_2, and I_3. The primed angles (i.e., ψ' and ψ_1') were used to represent initial positions. The Lagrangian approach was utilized to formulate the equations for this vehicle which has six degrees of freedom. The generalized coordinates were three translations (x, z, and w) and three rotations (θ_y, θ_v, and ψ).

Lagrange's equations can be expressed in general form as

$$\frac{d}{dt}\left(\frac{\partial L}{\partial \dot{q}_j}\right) - \frac{\partial L}{\partial q_j} + \frac{\partial RD}{\partial \dot{q}_j} = Q_j \qquad (2.1)$$

where

L = KE - PE;

RD = Rayleigh's dissipation function;

Q = generalized forces;

q = generalized coordinates;

KE = kinetic energy function;

PE = potential energy function; and

j = 1 - 6.

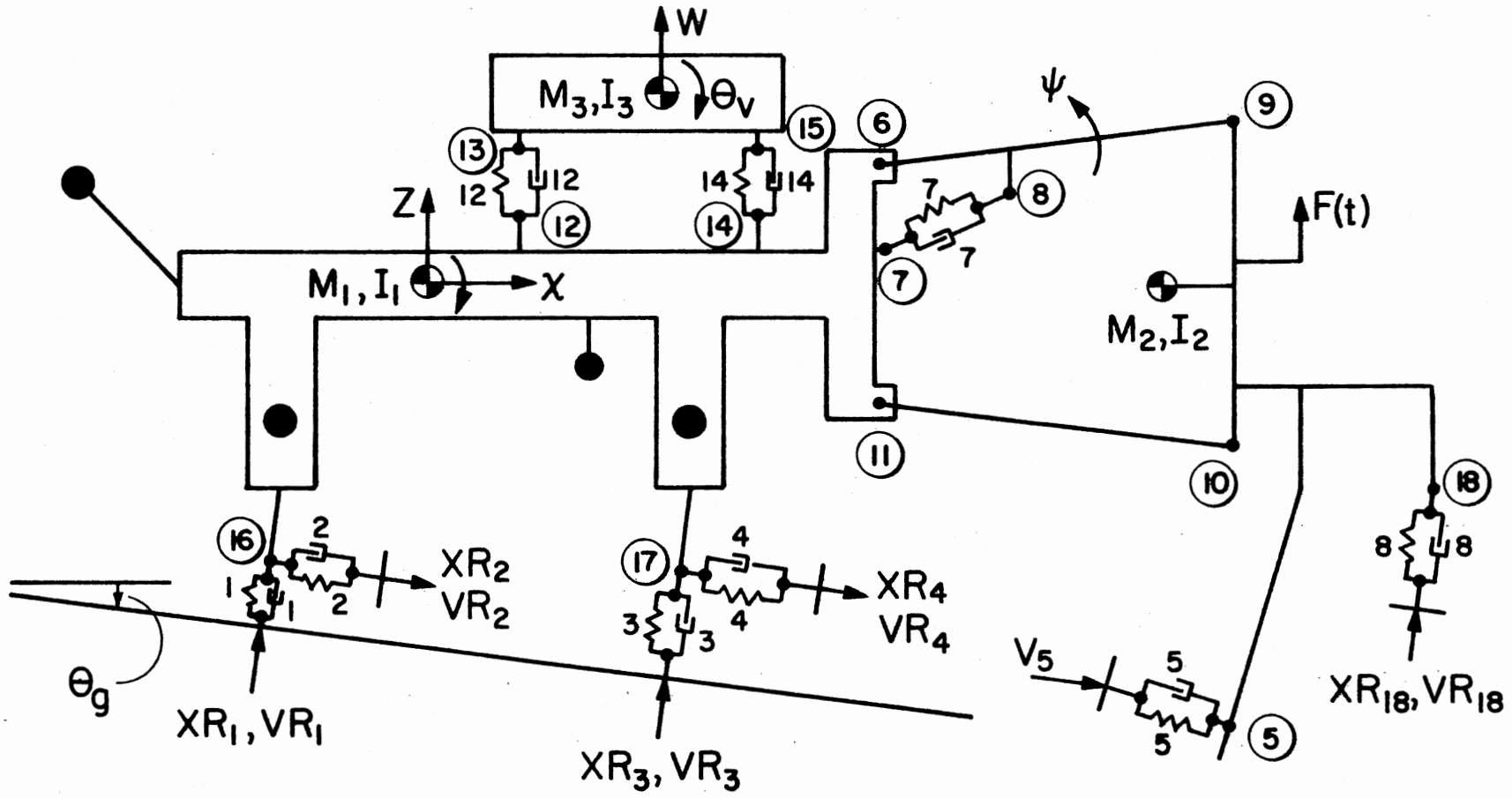

Figure 1. The 2-D Vehicle Model With Vibratory Plow

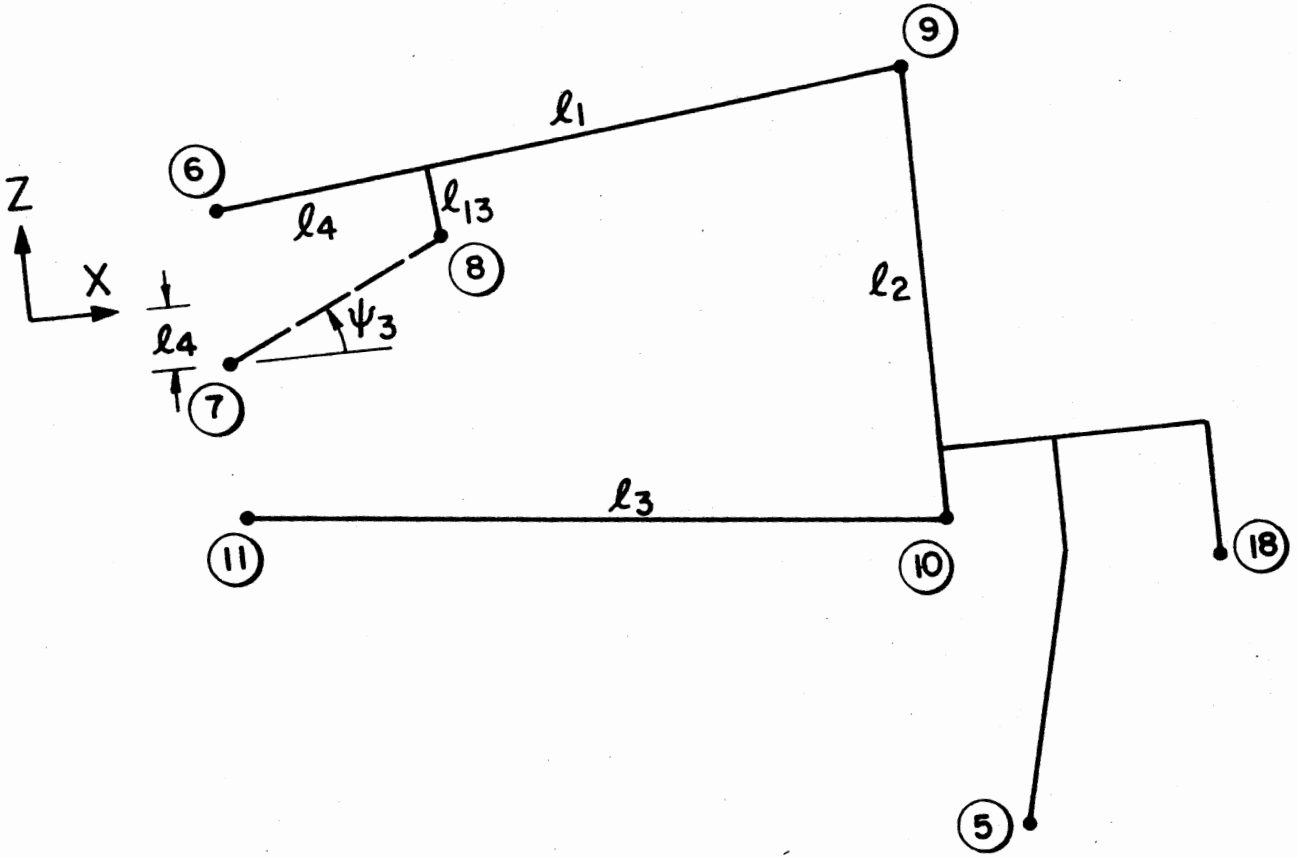

Figure 2. The Vibratory Plow Assembly Model

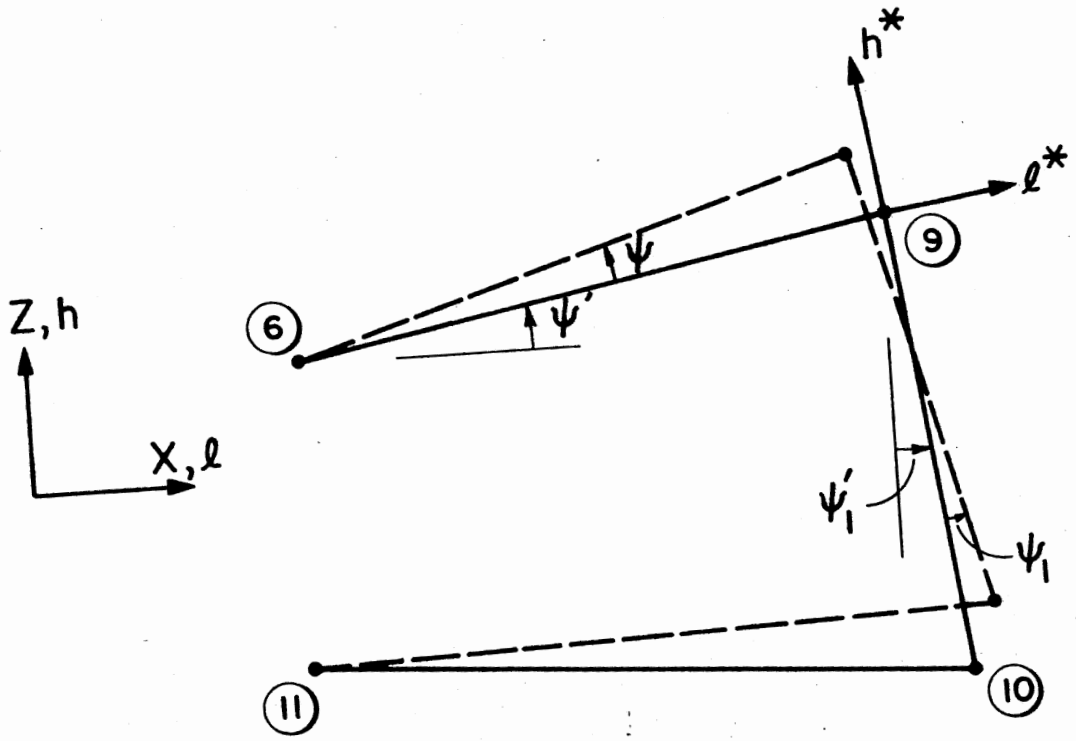

Figure 3. Angles Associated With the Plow Assembly

Substitution of L = KE - PE into Equation (2.1) yielded

$$\frac{d}{dt}\left(\frac{\partial KE}{\partial \dot{q}_j} - \frac{\partial PE}{\partial \dot{q}_j}\right) - \left(\frac{\partial KE}{\partial q_j} - \frac{\partial PE}{\partial q_j}\right) + \frac{\partial RD}{\partial \dot{q}_j} = Q_j \tag{2.2}$$

Equation (2.2) can also be written as

$$\frac{d}{dt}\left(\frac{\partial KE}{\partial \dot{q}_j}\right) - \frac{d}{dt}\left(\frac{\partial PE}{\partial \dot{q}_j}\right) - \frac{\partial KE}{\partial q_j} + \frac{\partial PE}{\partial q_j} + \frac{\partial RD}{\partial \dot{q}_j} = Q_j \tag{2.3}$$

The kinetic energy of the system was expressed as

$$KE = \frac{1}{2} M_1 VM_1^2 + \frac{1}{2} I_1 \omega_1^2 + \frac{1}{2} M_2 VM_2^2 + \frac{1}{2} I_2 \omega_2^2 + \frac{1}{2} M_3 VM_3^2 + \frac{1}{2} I_3 \omega_3^2 \tag{2.4}$$

where VM_1, VM_2, and VM_3 are translational velocities of the body c.g., and ω_1, ω_2, and ω_3 are rotational velocities about an axis through the body c.g. for bodies 1, 2, and 3, respectively.

A zero potential energy state must be established as a reference for the potential energy function. In this formulation the zero-state was taken as the position of the vehicle in equilibrium with its gravitational forces. Therefore, the vehicle weight did not appear in the potential energy function. This function for the model shown in Figure 1 was expressed as

$$\begin{aligned} PE = {} & \frac{1}{2} K_1 (XK_1 - XR_1)^2 + \frac{1}{2} K_2 (XK_2 - XR_2)^2 + \frac{1}{2} K_3 (XK_3 - XR_3)^2 \\ & + \frac{1}{2} K_4 (XK_4 - XR_4)^2 + \frac{1}{2} K_5 (XK_5)^2 + \frac{1}{2} K_7 (XK_8 - XK_7)^2 \\ & + \frac{1}{2} K_8 (XK_{18} - XR_{18})^2 + \frac{1}{2} K_{12} (XK_{13} - XK_{12})^2 \\ & + \frac{1}{2} K_{14} (XK_{15} - XK_{14})^2 \end{aligned} \tag{2.5}$$

where

XK_i = displacement of the ith spring element in terms of the generalized coordinates; and

XR_i = reference displacement of the ith spring element.

In a similar manner the dissipation function was expressed in terms of the velocity components:

$$RD = \frac{1}{2} C_1 (VC_1 - VR_1)^2 + \frac{1}{2} C_2 (VC_2 - VR_2)^2 + \frac{1}{2} C_3 (VC_3 - VR_3)^2 + \frac{1}{2} C_4 (VC_4 - VR_4)^2 + \frac{1}{2} C_5 VC_5^2 + \frac{1}{2} C_7 (VC_8 - VC_7)^2 + \frac{1}{2} C_8 (VC_{18} - VR_{18})^2 + \frac{1}{2} C_{12} (VC_{13} - VC_{12})^2 + \frac{1}{2} C_{14} (VC_{15} - VC_{14})^2 \quad (2.6)$$

where

VC_i = velocity of the ith damping element in terms of the generalized coordinates; and

VR_i = reference velocity of the ith damping element.

The generalized forces were obtained through the application of the Principle of Virtual Work. For this problem Q was expressed as

$$Q = f(\psi, F(t))$$

where the function f( ) was determined later in this development.

Displacements and Velocities

It was necessary to determine the displacements and velocities used in Equations (2.4) through (2.6) in terms of the generalized coordinates (x, z, w, θ_y, θ_v, ψ). These quantities were derived with reference to a fixed axis system at the zero potential state with unit vectors ℓ and n in the directions of X and Z, respectively.

Because the vibration in this study was observed to involve small amplitudes about some operating equilibrium position, the kinematic expressions were linearized. All product terms were neglected and the displacement angles were approximated as cos $\angle \rightarrow 1$ and sin $\angle \rightarrow \angle$.

The displacement of a point rigidly attached to the frame was expressed, in general, as

$$\Delta_i = [x + a_i\theta_y]\ell + [z + d_i\theta_y]n \tag{2.7}$$

where

a_i = X distance from the point to the frame c.g.; and

d_i = Z distance from the point to the frame c.g.

Correspondingly, the displacement of a point on the cab was written as

$$\Delta_i = [x + h_z\theta_y + d_i\theta_v]\ell + [w + a_i\theta_v]n \tag{2.8}$$

where

a_i = X distance from the point to the cab c.g.; and

d_i = Z distance from the point to the cab c.g.

The displacement of a point rigidly attached to link ℓ_2 of the four-bar plow linkage assembly was expressed as

$$\Delta_i = [x + T1_i\psi + T2_i\theta_y]\ell + [z + T3_i\psi + T4_i\theta_y]n \tag{2.9}$$

where the constants $T1_i$, $T2_i$, $T3_i$, and $T4_i$ were determined by the linkage geometry and the equilibrium position. Appendix A contains a complete derivation of Equation (2.9).

Point velocities were obtained by differentiating Equations (2.7) through (2.9) with respect to time:

$$V_i = [\dot{x} + a_i\dot{\theta}_y]\ell +]\dot{z} + d_i\dot{\theta}_y]n \tag{2.10}$$

$$V_i = [\dot{x} + h_z\dot{\theta}_y + d_i\dot{\theta}_v]\ell + [\dot{w} + a_i\dot{\theta}_v]n \tag{2.11}$$

$$V_i = [\dot{x} + Tl_i\dot{\psi} + T2_i\dot{\theta}_y]\ell + [\dot{z} + T3_i\dot{\psi} + T4_i\dot{\theta}_y]n \tag{2.12}$$

The mass of the plow assembly was assumed to all lie on link ℓ_2. Thus, the c.g. remained fixed with respect to link ℓ_2. This assumption allowed the total mass velocity to be given by Equation (2.12).

The velocities and displacements in terms of the generalized coordinates were substituted into the energy expressions and the equations of motion were formulated through the use of Equation (2.3). Differentiation before substitution simplified the development.

Kinetic Energy Derivatives

The kinetic energy expression, given by Equation (2.4), can also be expressed as

$$KE = \frac{1}{2} M_1 (VMX_1^2 + VMZ_1^2) + \frac{1}{2} I_1\omega_1^2 + \frac{1}{2} M_2 (VMX_2^2 + VMZ_2^2)$$
$$+ \frac{1}{2} I_2\omega_2^2 + \frac{1}{2} M_3 (VMX_3^2 + VMZ_3^2) + \frac{1}{2} I_3\omega_3^2 \tag{2.13}$$

Differentiation of Equation (2.13) with respect to $\dot{q}$ yielded

$$\frac{\partial KE}{\partial q_j} = M_1 [VMX_1 \frac{\partial VMX_1}{\partial \dot{q}_j} + VMZ_1 \frac{\partial VMZ_1}{\partial \dot{q}_j}] + I_1\omega_1 \frac{\partial \omega_1}{\partial \dot{q}_j}$$
$$+ M_2 [VMX_2 \frac{\partial VMX_2}{\partial \dot{q}_j} + VMZ_2 \frac{\partial VMZ_2}{\partial \dot{q}_j}] + I_2\omega_2 \frac{\partial \omega_2}{\partial \dot{q}_j}$$
$$+ M_3 [VMX_3 \frac{\partial VMX_3}{\partial \dot{q}_j} + VMZ_3 \frac{\partial VMZ_3}{\partial \dot{q}_j}] + I_3\omega_3 \frac{\partial \omega_3}{\partial \dot{q}_j} \tag{2.14}$$

Equation (2.14) represents the operation for all of the generalized coordinates. The scalar quantities (i.e., VMX_1, VMZ_1, etc.) were taken from

the velocity vectors which were previously given in general form.

After all generalized coordinates had been substituted into Equation (2.14), a set of six linear equations involving only velocity terms resulted. Differentiation of these equations in matrix form with respect to time yielded the mass matrix for the system. Thus,

$$\frac{d}{dt}\left(\frac{\partial KE}{\partial \dot{q}}\right) = [M]\{\ddot{q}\} \tag{2.15}$$

where

$$\{q\} = [\ddot{x}\ \ddot{z}\ \ddot{\theta}_y\ \ddot{\psi}\ \ddot{w}\ \ddot{\theta}_v]^T$$

Reference (20) contains the velocity vectors for the three masses, the six equations represented by Equation (2.14), and the coefficients of the system mass matrix.

Potential Energy Derivatives

Equation (2.5) represents the potential energy of the system. The four terms (XK_1, XK_2, XK_3, and XK_4) associated with wheel displacements and the bounce tire displacement XK_8 must be in the direction parallel to the spring elements. As shown in Figure 1, the ground and thus these spring elements were rotated an angle θ_g with respect to the fixed reference X-Z. Therefore, the spring displacements XK_i had to be expressed in terms of θ_g and the components of the displacement vector at each corresponding wheel. These displacements were written as

$$XK_i = \Delta X_i\ DCX_i + \Delta Z_i\ DCZ_i \tag{2.16}$$

where DCX_i and DXZ_i are direction cosines in the X and Z directions, respectively, and ΔX_i and ΔZ_i are scalar quantities from the displacement vectors given by Equations (2.7) and (2.9).

The spring displacement X_{K7} depends upon the relative displacement between points 7 and 8. It was also necessary to find the angle ψ_3 which the spring element makes with respect to the X-axis. Having found these, X_{K7} was expressed as

$$XK_7 = (\Delta X_8 - \Delta X_7)\cos\psi_3 - (\Delta Z_8 - \Delta Z_7)\sin\psi_3 \tag{2.17}$$

where ΔX_7, ΔZ_7, ΔX_8, and ΔZ_8 were taken from the displacement vectors. Appendix B contains the development of Equation (2.17) along with the relative displacements and the ψ_3 equation.

The displacements of the spring elements in Equation (2.15) were determined using Equations (2.7), (2.8), (2.9), (2.16), and (2.17). Equation (2.5) was written, in general, as

$$PE = \sum \frac{1}{2} K_i (XK_i - XR_i)^2 \tag{2.18}$$

The potential energy was then differentiated with respect to each generalized coordinate. This operation resulted in

$$\frac{\partial PE}{\partial q_j} = \sum K_i (XK_i - XR_i)\left[\frac{\partial XK_i}{\partial \Delta X_i}\frac{\partial \Delta X_i}{\partial q_j} + \frac{\partial XK_i}{\partial \Delta Z_i}\frac{\partial \Delta Z_i}{\partial q_j}\right] \tag{2.19}$$

Equation (2.19) represents a set of six linear equations involving spring constants, displacement components, and input reference displacements for the various spring elements. These equations written in matrix form yielded the stiffness matrix and a load vector associated with the reference displacements. This equation took the form of

$$\frac{\partial PE}{\partial q} = [K]\{q\} - \{FK\} \tag{2.20}$$

where

$$\{q\} = [x \; z \; \theta_y \; \psi \; w \; \theta_v]^T$$

Reference (20) contains the displacements represented by Equations (2.7), (2.8), (2.9), and (2.16) and the set of six equations given by Equation (2.19). The coefficients of the stiffness matrix [K] and the load vector {FK} are also given.

Dissipation Function Derivatives

The dissipation function represented by Equation (2.6) contains velocity terms which act parallel to the dashpot associated with the wheel and bounce tire models. Because the damping and spring elements were both rotated an angle θ_g with respect to the X-axis, the velocity components were defined by a set of equations similar to those of Equation (2.16). Thus,

$$VC_i = VX_i\ DCX_i + VZ_i\ DCZ_i \tag{2.21}$$

where VX_i and VZ_i are components of the velocity vectors given by Equations (2.10) and (2.12).

The relative velocity between points 7 and 8 was needed to evaluate the damping force in element 7. This velocity must be along a line rotated ψ_3 from the X-axis. Therefore, the velocity expression was similar to Equation (2.17) and was written as

$$VC_7 = (VX_8 - VX_7)\cos\psi_3 - (VZ_8 - VZ_7)\sin\psi_3 \tag{2.22}$$

where VX_7, VZ_7, VX_8, and VZ_8 were taken from the velocity vectors. Appendix B contains the derivation of Equation (2.22).

Equation (2.12) was used to evaluate the velocity of a point on the plow blade. However, the machine may also have a steady velocity component which is parallel to the ground. Therefore, the plow velocity was defined as

$$VC_5 = (VX_5 - VS\ \cos\theta_g)\ell + (VZ_5 + VS\ \sin\theta_g)n \tag{2.23}$$

where VS is the velocity component parallel to the ground and positive toward the front of the vehicle.

The dissipation function may be written, in general, as

$$RD = \sum \frac{1}{2} C_i (VC_i - VR_i)^2 \tag{2.24}$$

Equation (2.24) was differentiated with respect to the velocity of each generalized coordinate. This operation yielded

$$\frac{\partial RD}{\partial \dot{q}_j} = \sum C_i (VC_i - VR_i) \left[\frac{\partial VC_i}{\partial VX_i} \frac{\partial VX_i}{\partial \dot{q}_j} + \frac{\partial VC_i}{\partial VZ_i} \frac{\partial VZ_i}{\partial \dot{q}_j}\right] \tag{2.25}$$

A set of six equations involving damping coefficients, velocity components, and reference velocities is represented by Equation (2.25). These equations were written in matrix form to yield the damping matrix and a load vector associated with the reference velocities.

$$\frac{\partial RD}{\partial \dot{q}} = [C]\{\dot{q}\} - \{FC\} \tag{2.26}$$

The velocities represented by Equations (2.10), (2.11), (2.12), and (2.21) and the set of equations given by Equation (2.25) are presented in Reference (20). Also, the coefficients of the damping matrix [C] and the load vector {FC} are listed.

Generalized Forces

The Principle of Virtual Work was applied for each of the generalized coordinates to yield the generalized forces.

$$\delta WE_i = Q_i \delta q_i \tag{2.27}$$

The only external force during plowing was the rotating shaker force F(t). Therefore, the Q_i's were determined in terms of F(t) and the vehicle equilibrium position. They were expressed as

$$Q_1 = -F(t)\ \sin\psi_1'$$
$$Q_2 = F(t)\ \cos\psi_1'$$
$$Q_3 = F(t)\ TQ_3$$
$$Q_4 = F(t)\ TQ_4 \qquad (2.28)$$

where TQ_3 and TQ_4 are constants determined from the plow geometry and are given in Reference (20).

Equations of Motion

Two terms were still to be evaluated in Equation (2.3). The kinetic and potential energy functions of this development resulted in

$$\frac{\partial PE}{\partial q} \doteq 0 \qquad (2.29)$$

and

$$\frac{\partial KE}{\partial q} \doteq 0 \qquad (2.30)$$

Equations (2.15), (2.20), (2.26), (2.29), and (2.30) were substituted into Equation (2.3) which resulted in

$$[M]\{\ddot{q}\} + [C]\{\dot{q}\} - \{FC\} + [K]\{q\} - \{FK\} = Q$$

or

$$[M]\{\ddot{q}\} + [C]\{\dot{q}\} + [K]\{q\} = \{Q + FC + FK\} \qquad (2.31)$$

Equation (2.31) represents the equations of motion for the six degree of freedom system written in matrix form. This system included the frame, cab, and vibratory plow assembly. The equations of motion

were also obtained for the digging chain attachment, which is shown in Figure 4. Because the frame and cab remain unchanged, Equation (2.31) was modified relatively easily for the digging chain.

Digging Chain Effects

The degree of freedom ψ was eliminated from the system because the digging chain boom was assumed to be rigidly attached to the frame. Therefore, the displacement of point 5, for this case, was given by Equation (2.7). Thus, the expressions for XK_5 and VC_5 were modified accordingly and the indicated operations performed again. The chain has no bounce tires or lift cylinder, so K_7, C_7, K_8, and C_8 were all set equal to zero. These changes yielded the proper stiffness and damping matrix for the system.

The mass matrix was also modified by setting both M_2 and I_2 equal to zero. The mass and inertia of the digging chain attachment was included in the vehicle frame body itself.

A new load matrix $\{Q\}$ had to be found for the digging chain. The total load caused by the digging action was applied to the frame at point 6 as shown in Figure 4. By definition, RCH is the total force in the chain and RMCH is the moment applied to the connecting point.

$$RMCH = RCH\ \ell_2 \tag{2.32}$$

Equation (2.27) again yielded

$$\begin{aligned} Q_1 &= RCH\ \cos\theta_{ch} \\ Q_2 &= -RCH\ \sin\theta_{ch} \\ Q_3 &= -RMCH + RCH(d_6\ \cos\theta_{ch} + a_6\ \sin\theta_{ch}) \end{aligned} \tag{2.33}$$

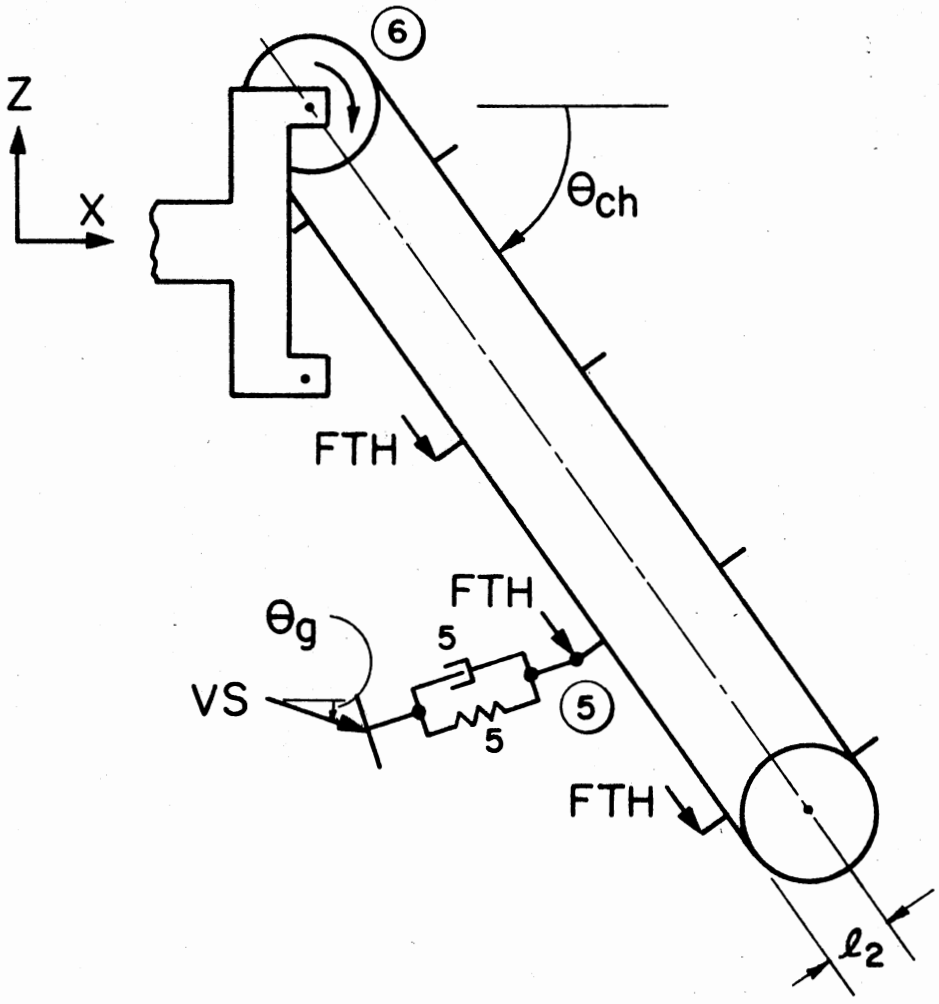

Figure 4. The Digging Chain Model

After the changes were made in the mass, stiffness, and damping matrices and the new load matrix introduced, Equation (2.31) was used for the digging chain equations of motion, where

$$\{q\} = [x \; z \; \theta_y \; w \; \theta_v]^T \tag{2.34}$$

The displacement vector for point 5 and the coefficients of [M], [K], and [C] are given in Reference (20).

Vehicle Geometry

The dimensions used in deriving the equations of motion were all measured with respect to the vehicle c.g. It is convenient to calculate the c.g. location because the vehicle frame mass is composed of an arbitrary number of concentrated masses rigidly attached to the frame plus a uniform distribution of the frame itself. After the c.g. location and the other geometry were known with respect to a common reference, the dimensions in the formulation were defined as

$$a_i = e_i - XCG$$

and

$$d_i = g_i - ZCG \tag{2.35}$$

where e_i and g_i are with respect to the reference. Appendix C contains the c.g. location and moment of inertia equations for the frame.

Soil-Structure Interaction

The ground stiffness and damping coefficients are denoted as K_5 and C_5, respectively. Due to movement of the blade in penetrated and unpenetrated soil, these values were not assumed to be constant. Therefore,

K_5 and C_5 were made to vary depending upon the position of the blade point and the unpenetrated soil line.

If x of the blade point is less than x of the soil line, then the blade is cutting and the coefficients were used at full value. However, when the blade backs away and is moving in already penetrated soil, the coefficients are reduced. Thus,

$$RK_5 = K_5 \ REK$$

and

$$RC_5 = C_5 \ REC \tag{2.36}$$

where REK and REC are reduction factors and may range in value from zero to one. The unpenetrated soil line moves at a constant velocity in the positive X-direction between cutting cycles.

The plow blade force is dependent upon the ground coefficients and the position of point 5. This was assumed to be the point of application for the resultant blade force. Equations (2.9) and (2.23) give the displacement and velocity of point 5. The force was expressed in vector form as

$$RPF = [\Delta X_5 \ RK_5 + (VX_5 - VS \cos\theta_g)RC_5]\ell + [\Delta Z_5 \ RK_5 + (VZ_5 + VS \sin\theta_g)RC_5]n \tag{2.37}$$

or

$$RPF = RPFX \ \ell + RPFZ \ n$$

The magnitude of the force vector was defined as

$$RPFM = \sqrt{RPFX^2 + RPFZ^2} \tag{2.38}$$

The angle (ϕ) through which the resultant ground force acts on the blade was found from Equation (2.37). This angle is defined as zero in the

positive X-direction and is measured positive in a clockwise rotation from that axis.

$$\phi = -\tan^{-1}[RPFZ/ARPFX] + \pi \qquad RPFX > 0$$

$$\phi = \tan^{-1}[RPFZ/ARPFX] \qquad RPFX < 0$$

$$\phi = \pi[RPFZ/ARPFZ]/2 \qquad RPFX = 0 \qquad (2.39)$$

For the digging chain attachment the ground coefficients also vary. The frame motion may cause the cutting teeth on the chain to back away from the soil just as the plow blade does. Again point 5 was denoted as the point of application for the resultant boom force. The modified displacement and velocity vectors for the digging chain as described earlier in this development were used to vary the ground coefficients in the same manner as for plowing. Therefore, Equations (2.36) through (2.39) were used to evaluate the magnitude and direction of the resultant boom force.

Not only the boom force but also the chain force is displacement-dependent. If the cutting teeth back away from the soil, then the individual tooth force must be reduced. Having the tooth force (FTH), the total chain force was expressed as

$$RCH = FTH\ NTD \qquad (2.41)$$

where NTD is the number of teeth which are digging. However, NTD is not a constant but depends on tooth spacing, depth of cut, and position of the chain. The complete derivation of Equation (2.41) is given in Appendix D. Because RCH appears in Equation (2.33), the load matrix for this case, the forcing function is both time- and position-dependent.

Tire Forces

The equations of motion represented by Equation (2.31) were solved

to yield the displacements, velocities, and accelerations of the generalized coordinates. These time-dependent vectors were then used to evaluate the tire and frame forces.

Each tire has a normal force and a tractive force. The displacements and velocities for the tire elements were given by Equations (2.16) and (2.21), respectively. These quantities along with the stiffness and damping coefficients resulted in

$$TF_i = [XK_i - XR_i]K_i + [VC_i - VR_i]C_i + SF_i \tag{2.42}$$

where

TF_i = normal or tractive force depending upon the element; and

SF_i = static force determined from the equilibrium position.

It should be noted that for this 2-D case, Equation (2.42) actually represents the forces in two tires acting in parallel.

Frame Loads

The frame is loaded at various points by force systems resulting from tire forces, cab forces, and the acceleration of the added masses. The tire forces were given by Equation (2.42). These were expressed as an equivalent force system applied to the frame directly above the front and rear axles. The equations are not given here but are contained in Reference (20).

The cab forces were calculated from Equations (2.7), (2.8), (2.10), and (2.11). For small displacements only the Z-component of the vectors must be used for the vertical forces. Therefore, the front vertical force was written as

$$FCFZ = (\Delta Z_{13} - \Delta Z_{12})K_{12} + (VZ_{13} - VZ_{12})C_{12} - WTZX + FCSZ \tag{2.43}$$

where

$$WTZX = M_3[\ddot{x}(d_{20} - d_{12}) - \ddot{x}(d_{14} - d_{12})/2 + \ddot{\theta}_y d_{20}]/(a_{14} - a_{12})$$

and FCSZ is the static force determined from the equilibrium position. A similar equation exists for the rear force. Because no relative motion was allowed between the cab and frame in the X-direction, a horizontal connecting force is created when the cab c.g. is accelerated. Thus, the front horizontal force was expressed as

$$FCFX = M_3(\ddot{x} + \ddot{\theta}_y d_{20})/2 \tag{2.44}$$

The total force was assumed to be equally distributed between the front and rear connections. Therefore, Equation (2.44) holds for the rear also.

Each concentrated mass has a location (XM_i, ZM_i) with respect to the frame c.g. and an attachment point (XIC_i, ZIC_i). The acceleration of any mass was expressed as

$$AM_i = (\ddot{x} + ZM_i\ddot{\theta}_y)\ell + (\ddot{z} - XM_i\ddot{\theta}_y)n \tag{2.45}$$

The mass was considered as a free body having known accelerations and unknown connecting forces. Newton's laws yielded three equations which were solved for the forces. These forces were written as

$$\begin{aligned} FCX_i &= -CCM_i(\ddot{x} + ZM_i\ddot{\theta}_y) \\ FCZ_i &= -CCM_i(\ddot{z} - XM_i\ddot{\theta}_y) \\ FCM_i &= FCX_i(ZIM_i - ZIC_i) - FCZ_i(XIM_i - XIC_i) - CCI_i\ddot{\theta}_y \end{aligned} \tag{2.46}$$

Stress Resultants

There are three stress resultants (SRX_i, SRZ_i, and $SRMY_i$) which must be determined at each output point. These resultants were written in

terms of the frame connecting forces and the inertia loading of the distributed frame.

Three different sets of equations had to be defined for the distributed loading. The output point location determines which set to use for the resultants. The three regions are

1. Point lies in front of the c.g.
2. Point lies behind the c.g. but on the uniform frame section.
3. Point lies beyond the uniform frame section.

Reference (20) contains the distributed loading equations for each region. For this development the axial, shear, and moment loading were denoted as SRXD, SRZD, and SRMYD, respectively.

The stress resultants at any output point were expressed as

$$\begin{aligned} SRX_i &= -\sum FCX_j + SRXD \\ SRZ_i &= -\sum FCZ_j + SRZD \\ SRMY_i &= \sum FCM_j + \sum FCX_j(ZIC_i - ZOP_i) + \sum FCZ_j(XOP_i - XIC_i) \\ &\quad + SRMYD \end{aligned} \tag{2.47}$$

where (XOP_i, ZOP_i) represent the location of the output point. The summations in Equation (2.47) include only the attachment points which lie in front of the output point. It should also be noted that the tire and cab forces have been included in the connecting forces. The stress resultants in Equation (2.47) are for the total frame and should be divided by two if they are applied to one side.

CHAPTER III

DEVELOPMENT OF THE THREE-DIMENSIONAL CASE

Lagrangian Formulation

The equations of motion for the 3-D model were also derived using a Lagrangian approach. The model is shown in Figures 5 through 8. Both the digging chain and vibratory plow were included. M_1, M_2, M_3, and M_4 denote the mass of the frame assembly, plow assembly, operator cab, and front axle, respectively. The inertia matrices for the corresponding bodies were denoted as $[I_1]$, $[I_2]$, $[I_3]$, and $[I_4]$. A model of the digging chain was shown in Chapter II and is not presented again in this section.

The tires and cab mounts were modeled as combinations of spring and damping elements which are oriented in three mutually perpendicular directions. For convenience only the spring elements are shown and numbered in Figures 5 through 8. There exists for every spring element having a stiffness K_i, a parallel damping element having a coefficient C_i. The front wheel steering angle (δ_F) and the rear wheel steering angle (δ_R) were treated as constants but not limited to small rotations. The dimensions of the plow assembly were the same as those used in the 2-D case. However, some of the points on the model have been renumbered. The angle α' was used to denote the initial position of the plow boom.

For the 3-D model a total of 15 degrees of freedom was allowed. The generalized coordinates associated with each body are listed in Table I. The general form of Lagrange's equation was given in the previous chapter.

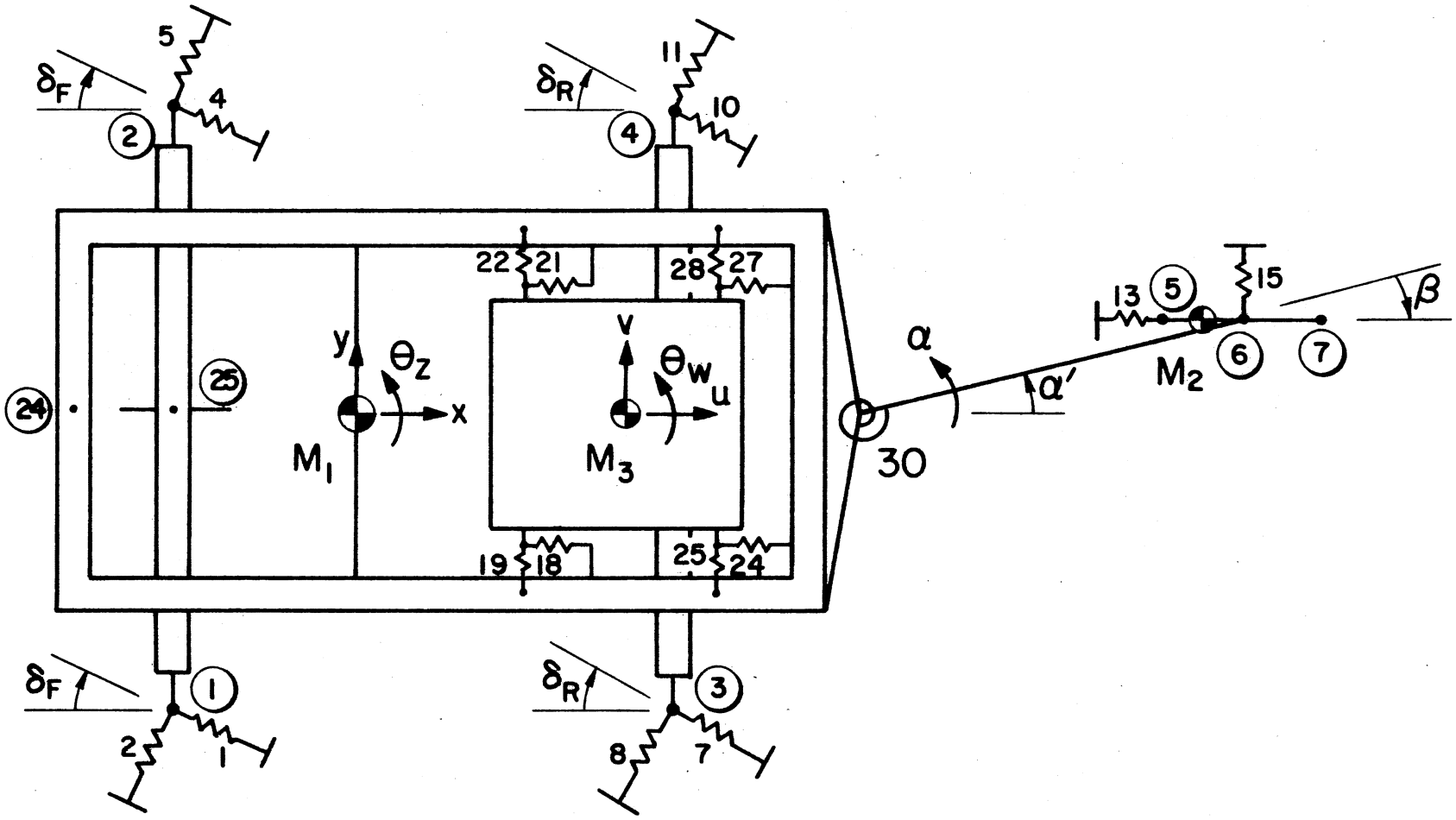

Figure 5. The 3-D Vehicle Model With Vibratory Plow in the X-Y Plane

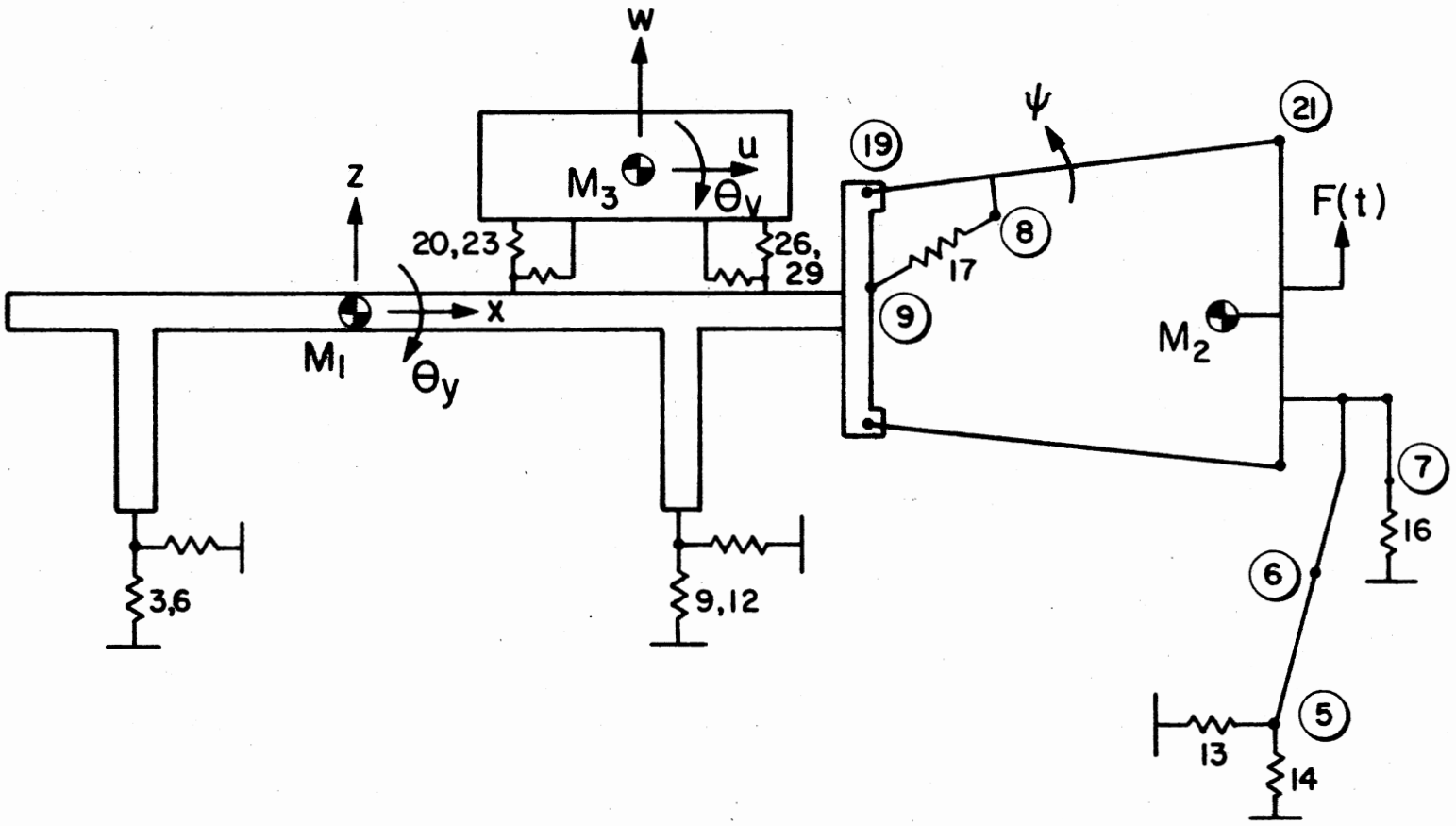

Figure 6. The 3-D Vehicle Model With Vibratory Plow in the X-Z Plane

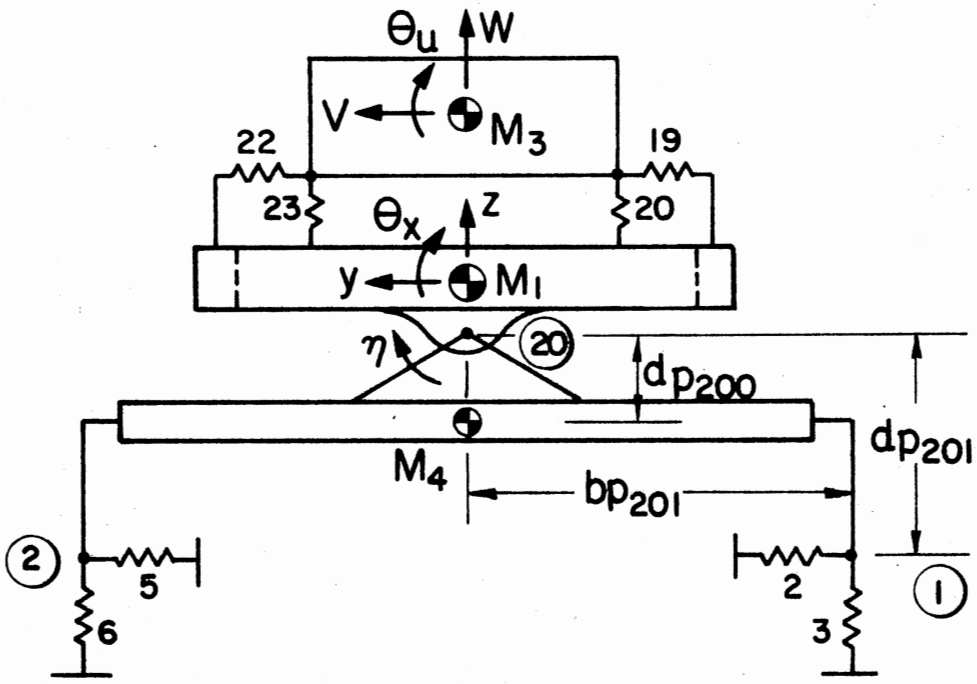

Figure 7. The Cab, Frame, and Front Axle Assembly in the Y-Z Plane

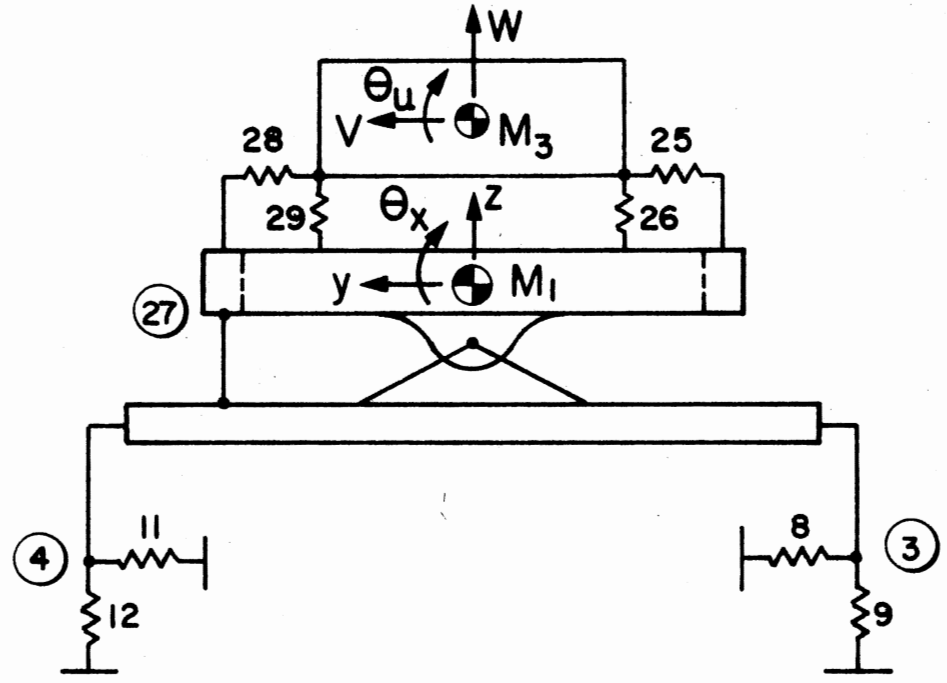

Figure 8. The Cab, Frame, and Rear Axle Assembly in the Y-Z Plane

TABLE I

DEGREES OF FREEDOM FOR THE 3-D MODEL

Body	Translations	Rotations
Frame Assembly	x, y, z	$\theta_x, \theta_y, \theta_z$
Cab Assembly	u, v, w	$\theta_u, \theta_v, \theta_w$
Front Axle	none	η
Vibratory Plow	none	ψ, α
Digging Chain	none	none

TABLE II

GENERALIZED ROTATIONAL VELOCITY COMPONENTS
FOR THE FOUR BODIES

Body	ωX_i	ωY_i	ωZ_i
Frame Assembly	$\dot{\theta}_x$	$\dot{\theta}_y$	$\dot{\theta}_z$
Cab Assembly	$\dot{\theta}_u$	$\dot{\theta}_v$	$\dot{\theta}_w$
Front Axle	$\dot{\eta}$	$\dot{\theta}_y$	$\dot{\theta}_z$
Plow Assembly	$\cos\alpha' \dot{\theta}_x + \sin\alpha' \dot{\theta}_y$	$-(CB-1)\sin\alpha' \dot{\theta}_x + (CB-1)\cos\alpha' \dot{\theta}_y + CB \dot{\psi}$	$\dot{\alpha}$

This development followed the same basic procedure as that used in Chapter II. Therefore, some of the details have been omitted to avoid repetition.

The kinetic energy of the system was expressed as

$$KE = \frac{1}{2}\bar{M}_1 VM_1^2 + \frac{1}{2}\omega_1^T [\bar{I}_1]\omega_1 + \frac{1}{2}M_2 VM_2^2 + \frac{1}{2}\omega_2^T [I_2]\omega_2$$
$$+ \frac{1}{2}M_3 VM_3^2 + \frac{1}{2}\omega_3^T [I_3]\omega_3 + \frac{1}{2}M_4 VM_4^2 + \frac{1}{2}\omega_4^T [I_4]\omega_4 \qquad (3.1)$$

where VM_1, VM_2, VM_3, and VM_4 represented the translational velocities of bodies 1, 2, 3, and 4, respectively, and ω_1, ω_2, ω_3, and ω_4 were the corresponding rotational velocities. Each of these velocities had to be expressed in terms of the generalized coordinates. $[\bar{I}_1]$ and $\bar{M}_1$ denote modified values because of the front axle degree of freedom.

As in the 2-D case, the zero potential energy state was taken to be the position at which the vehicle was in static equilibrium with the forces due to gravity. The potential function for the 3-D model was written as Equation (2.18), where XK_i and XR_i were defined previously. Correspondingly, the dissipation function was expressed as Equation (2.24), where VC_i and VR_i were defined previously.

Again, the generalized forces were obtained by applying the Principle of Virtual Work. This was done for each of the generalized coordinates. Thus, Equation (2.27) was used.

All displacements and velocities in the potential and dissipation functions were defined in terms of the generalized coordinates. A linear formulation of the problem was made because the displacements of the actual system were observed to fall within the range of linear theory.

Displacements and Velocities

The position vector of any point on the frame was expressed in the fixed axis system as

$$\rho_i = a_i \ell + b_i m + d_i n \tag{3.2}$$

where ℓ, m, and n are unit vectors in the X, Y, and Z directions, respectively. The components a_i, b_i, and d_i represent the distances from the body c.g. or axis origin to the ith point. Therefore, the displacement of any point on the frame could be expressed as

$$\begin{aligned}\Delta_i = &(x + \bar{d}_i\theta_y - b_i\theta_z)\ell \\ &+ (y + \bar{a}_i\theta_z - d_i\theta_x)m \\ &+ (z + b_i\theta_x - a_i\theta_y)n\end{aligned} \tag{3.3}$$

where $\bar{d}_i$ and $\bar{a}_i$ were used to denote the distances from the center of mass to the point where rotation occurred about the Y-axis. Because the front axle had only one degree of freedom relative to the frame, the frame assembly and front axle rotate as one rigid body in the X-Z plane.

The displacement of a point on the front axle was defined by introducing its rotational freedom η. The dimensions are shown in Figure 7. The relative displacement of point 1 with respect to point 20 was combined with Equation (3.3) to yield

$$\begin{aligned}\Delta_1 = &[x + (\bar{d}_{20} - dp_{201})\theta_y - (b_{20} - bp_{201})\theta_z]\ell \\ &+ [y + a_{20}\theta_z - d_{20}\theta_x + dp_{201}\eta]m \\ &+ [z + b_{20}\theta_x - \bar{a}_{20}\theta_y - bp_{201}\eta]n\end{aligned} \tag{3.4}$$

A similar equation exists for point 2 and can be found in Reference (20).

Displacements of points which lie on the plow blade (i.e., 5 and 6) were somewhat more difficult to obtain because of the four-bar linkage and the two degrees of freedom associated with the plow assembly. It was convenient to define the displacement of point 21 and then the displacements of all points on the blade were obtained relative to point 21. The displacements were expressed, in general, as

$$\begin{aligned}\Delta_i = {} & [x + RIY_i\theta_y - b_{19}\theta_z + RIX_i\theta_x + RIS_i\psi - TB_1\alpha]\ell \\ & + [y + RJZ_i\theta_z + RJX_i\theta_x + RJY_i\theta_y + RJS_i\psi + TA_1\alpha]m \\ & + [z + RKX_i\theta_x + RKY_i\theta_y + RKS_i\psi] \end{aligned} \tag{3.5}$$

where the constants were defined in terms of plow geometry and point location on the blade. Appendix E contains a complete derivation of Equation (3.5) and all of the constants are given in Reference (20).

Point 8 was used to represent the lift cylinder connection to the upper plow-arm. The total displacement was found by combining Equation (3.3) (for point 19) with the displacement of point 8 with respect to point 19. Thus, the displacement was expressed as

$$\begin{aligned}\Delta_8 = {} & [x + \bar{d}_{19}\theta_y - b_{19}\theta_z - TD_8\psi - TB_8\alpha]\ell \\ & + [y + a_{19}\theta_z - (d_{19} + TD_8)\theta_x + TA_8\alpha]m \\ & + [z + (b_{19} + TB_8)\theta_x - \bar{a}_{19}\theta_y + TA_8\psi]n \end{aligned} \tag{3.6}$$

where the constants TA_8, TB_8, and TD_8 depend on the plow geometry and are listed in Reference (20).

The displacement of points on the cab was determined with respect to the generalized coordinates associated with its motion. A fixed axis system U, V, and W, which had its origin at the cab c.g., was used. Because the U, V, and W axis system was parallel to the X, Y, and Z system, the

unit vectors ℓ, m, and n were used for the cab point displacements also. Therefore, the displacement of any point on the cab was written as

$$\begin{aligned}\Delta_i = &[u + d_i\theta_v - b_i\theta_w]\ell \\ &+ [v + a_i\theta_w - d_i\theta_u]m \\ &+ [w + b_i\theta_u - a_i\theta_v]n\end{aligned} \tag{3.7}$$

where a_i, b_i, and d_i are components of the position vector with respect to the cab c.g.

Thus, equations were obtained for the displacement of all points on the vehicle model with respect to the fixed axis systems. Because these equations were observed to be linear with respect to the generalized coordinates, the velocities of those corresponding points were obtained by replacing the displacement coordinates with their first time-derivatives.

Energy and Dissipative Function Derivatives

Equation (3.1) expressed the kinetic energy in terms of the translational velocities which, in turn, were written as

$$VM_i^2 = VMX_i^2 + VMY_i^2 + VMZ_i^2 \tag{3.8}$$

where VMX_i, VMY_i, and VMZ_i are components of the velocity vector associated with the center of mass for the ith body. The rotational velocity (ω_i) represented a column matrix of velocities about the three major axes of the body. Thus, ω_i, in general, was written as

$$\omega_i = [\omega X_i \ \omega Y_i \ \omega Z_i]^T \tag{3.9}$$

The rotational velocities associated with each of the four bodies along their major axes are listed in Table II (see page 31).

For each of the bodies the inertia values were given with respect to the center of mass. In bodies 1, 3, and 4 the major axes were chosen parallel to the X, Y, and Z axis system. Because of the front axle, $[I_1]$ and M_1 had to be modified and were denoted as $[\bar{I}_1]$ and $\bar{M}_1$. A complete derivation of the modified terms are given in Appendix F. For the plow assembly it was convenient to define the inertia properties with respect to the plane of the boom. The $[I_2]$ matrix was set up for the x-x axis to lie in the boom plane and the z-z axis to be vertical passing through point 21. Therefore, the inertia matrix for the plow assembly was dependent upon the equilibrium position ψ' and the constant angle β.

It was assumed that bodies 3 and 4 were symmetric with respect to the X-Z plane. This implied that IXY and IYZ, for those two bodies, were zero. Equation (3.1) was written in summation form and differentiated with respect to the generalized velocity $\dot{q}$. This yielded

$$\begin{aligned}\frac{\partial KE}{\partial \dot{q}_j} = &\sum_{i=1}^{4} M_i \left(VMX_i \frac{\partial VMX_i}{\partial \dot{q}_j} + VMY_i \frac{\partial VMY_i}{\partial \dot{q}_j} + VMZ_i \frac{\partial VMZ_i}{\partial \dot{q}_j}\right) \\ &+ \sum_{i=1}^{4} \left(IXX_i \omega X_i \frac{\partial \omega X_i}{\partial \dot{q}_j} + IYY_i \omega Y_i \frac{\partial \omega Y_i}{\partial \dot{q}_j} + IZZ_i \omega Z_i \frac{\partial \omega Z_i}{\partial \dot{q}_j}\right. \\ &\left. + IXZ_i \omega X_i \frac{\partial \omega Z_i}{\partial \dot{q}_j} + IXZ_i \omega Z_i \frac{\partial \omega X_i}{\partial \dot{q}_j}\right) \\ &+ \sum_{i=1}^{2} \left(IXY_i \omega X_i \frac{\partial \omega Y_i}{\partial \dot{q}_j} + IXY_i \omega Y_i \frac{\partial \omega X_i}{\partial \dot{q}_j}\right. \\ &\left. + IYZ_i \omega Y_i \frac{\partial \omega Z_i}{\partial \dot{q}_j} + IYZ_i \omega Z_i \frac{\partial \omega Y_i}{\partial \dot{q}_j}\right) \qquad (3.10)\end{aligned}$$

The scalar velocity values in Equation (3.10) were taken from the velocity vectors for the center of masses. These vectors are given in Reference (20).

The matrix of generalized coordinates can be written as

$$\{q\} = [x\ y\ z\ \theta_x\ \theta_y\ \theta_z\ u\ v\ w\ \theta_u\ \theta_v\ \theta_w\ \eta\ \psi\ \alpha]^T \tag{3.11}$$

Each generalized coordinate was substituted into Equation (3.10) which yielded a set of 15 linear equations involving the velocity terms. Differentiating these equations with respect to time and writing them in matrix form yielded the mass matrix. Reference (20) contains the coefficients of the matrix.

The potential energy of the system was expressed as Equation (2.18). The spring elements were numbered and the scalar displacement quantities were taken from the vector displacement equations. In accordance with Equation (2.3), the potential energy was differentiated with respect to the generalized coordinates. This resulted in Equation (2.19). Each coordinate was substituted into Equation (2.19) which resulted in a set of 15 linear equations. These were written in matrix form and resulted in the stiffness matrix and an associated load matrix. All displacement expressions, the set of linear equations, and the coefficients of the two matrices are given in Reference (20).

The dissipation function was expressed by Equation (2.24) which has the same form as Equation (2.18), where K_i, XK_i, and XR_i were replaced by C_i, VC_i, and VR_i, respectively. The velocity term VC_i represented the time derivative of the displacement function XK_i. These expressions were readily obtained from the equations listed in Reference (20).

Equation (2.24) was differentiated with respect to the generalized velocity term and written in matrix form to yield the damping matrix and

an associated load matrix. These matrices had the same form as those developed for the stiffness terms. Therefore, the damping matrix and its load matrix were evaluated by replacing the stiffness terms with damping terms in the previously derived stiffness associated matrices.

Generalized Forces

The generalized forces Q_i were evaluated by invoking the Principle of Virtual Work. The only external load for the plow assembly was the rotating shaker force which acted through point 22 on the plow blade. This force vector was denoted as F_A and the displacement vector as Δ_{22}. Thus, the work done by the external force was

$$WE = F_A \cdot \Delta_{22} \tag{3.12}$$

The first variation of Equation (3.12) yielded Equation (2.27). This equation applied for each coordinate and resulted in the generalized load matrix {Q}. Reference (20) contains the load matrix.

Having the mass, stiffness, damping, and load matrices, the equations of motion were written as Equation (2.31).

Digging Chain Effects

The previous development was made for the model with a vibratory plow. Equations were also written for the vehicle and digging chain model. The two degrees of freedom, associated with the plow assembly, ψ and α were eliminated. The digging chain was assumed to be always parallel to the X-Z plane, but could be offset from the center of the vehicle.

The displacement of points on the digging chain was determined from Equation (3.5) by dropping the ψ and α terms and redefining the constants.

Therefore, the stiffness and damping matrices were modified indirectly through the change in the constant values. Because the digging chain had no lift cylinder, bounce tires, or rotational spring element, the values of K_{16}, K_{17}, and K_{30} and the corresponding damping terms were set equal to zero. The mass matrix was modified by setting M_2 and the inertia matrix I_2 both equal to zero. Also, α' and β were defined to be zero.

The final change made for the digging chain model was the load matrix. A resultant force (RCH) and moment (RMCH) were applied to the frame at point 19. These loads were the same as described in Chapter II. The load matrix was developed by combining Equation (3.3) for the displacement of point 19 and the external loads along with the Principle of Virtual Work. This matrix is given in Reference (20).

Vehicle Geometry and Soil-Structure Interaction

All dimensions in the equations of motion were taken with respect to the c.g. of the respective bodies. It was observed to be convenient to use a known fixed reference point to input all vehicle geometry. The c.g. locations were also supplied and then equations such as Equation (2.35) were used to calculate the required dimensions.

As in the 2-D case, the ground coefficients were not constant due to the plowing and digging actions. These coefficients were varied in the same manner as described in Chapter II. Of course, the displacements for the model were found from the 3-D equations. For this case only the components of the plow and digging boom force vectors were found and not the total magnitude and direction. The individual tooth and resultant chain forces were calculated the same way for the 2-D and 3-D cases.

Spring and Damping Element Forces

The equations of motion were solved for the rigid body displacements, velocities, and accelerations. The forces in the spring and damping elements were evaluated as

$$FS_i = (XK_i - XR_i)K_i \tag{3.13}$$

$$FD_i = (VC_i - VR_i)C_i \tag{3.14}$$

Finally, the tire, plow, and cab-mount forces were obtained by combining Equations (3.13) and (3.14) for the proper set of spring and damping elements.

Frame Loads

The frame structure for the 3-D model was analyzed with a general purpose structural program. Thus, the time-dependent frame loads at selected points were found. These points were chosen where the major loads are applied to the frame. They are caused by the reel and reel carrier, front and rear axles, and the operator cab connecting points and are numbered 24, 25, 26, 27, 28, 29, 30, and 31, respectively.

The reel and reel carrier were assumed to be rigidly attached to the frame. This allowed the acceleration of the center of mass to be calculated in terms of the rigid body accelerations. Then, frame connecting forces were found by writing the equations of motion for the isolated reel and reel carrier system. Newton's Laws of Motion were applied to the system which yielded the six frame loads FX_{24}, FY_{24}, FZ_{24}, TX_{24}, TY_{24}, and TZ_{24}. The derivation of these equations and other frame loads was straightforward and thus omitted from this thesis. (However, all frame load equations appear in Reference (20).) The forces FX, FY, and

FZ are positive in the directions of the positive coordinate axes. Also, the moments TX, TY, and TZ are positive using the same sign convention and the right-hand rule.

The front axle is shown in Figure 7. It was modeled to be pin-connected at point 20 and not to produce a moment, TX. The equations of motion were written about the axle center of mass and rearranged to yield the frame loads. These expressions involved the front tire forces, front steering angle, accelerations, and front axle inertia properties.

Figure 8 shows the rear axle assembly. The geometric properties, weights, etc. are identical to those of the front axle. Although the rear axle is pin-connected to the frame, a leveling cylinder prevents relative rotation between the frame and axle about the pin. Again TX was zero; however, the lift cylinder force FZ_{27} was found. Thus, a set of six equations resulted involving the rear tire forces, rear steering angle, accelerations, and rear axle inertia properties.

The cab-mount forces were found and then applied to the frame at points 28, 29, 30, and 31. These forces were expressed for each element by Equations (3.13) and (3.14). For example, the force in the mount in the X-direction at point 10 was

$$FX_{10} = -(FS_{18} + FD_{18}) \tag{3.15}$$

where FS_{18} and FD_{18} are given by Equations (3.13) and (3.14). Correspondingly, FY_{10} and FZ_{10} were found in a similar manner using the properly numbered elements. These forces were then transferred to an arbitrarily located output point 28 where three forces and three resulting moments were applied to the frame. Loads at points 29, 30, and 31 were obtained in the same manner.

CHAPTER IV

NUMERICAL SOLUTION

As shown in the previous two chapters, each model was described by a set of second-order, linear differential equations. The 2-D system has 6 equations and the 3-D system has 15 equations. Separate programs were written for the two models because a shorter version was developed for the case of plane motion. The 2-D model requires less input and the complete frame analysis is included. Although the form of the final results from the two programs is different, the basic structure and logic are the same.

Both programs were coded in FORTRAN IV and were executed on the Oklahoma State University's IBM 370/158 computer system. Both programs can perform free and/or forced vibration analyses. For the free vibration analysis the mass and stiffness matrices were generated and the eigenvalues and eigenvectors were extracted using two standard SSP subroutines (NROOT and EIGEN). This was the classical eigenvalue approach and no damping was included for free vibrations.

The forced-vibration response was obtained by direct integration of the equations of motion. This numerical integration was performed using a Runge-Kutta fourth-order technique. The damping matrix was included for the forced vibration. Either set of the equations of motion were written in general form as

$$[M]\{\ddot{q}\} + [C]\{\dot{q}\} + [K]\{q\} = \{R\} \tag{4.1}$$

This second-order matrix equation was expressed as two first-order

equations simply by introducing a new matrix {P}. Thus, defining

$$\{\dot{q}\} = \{P\} \tag{4.2}$$

and substituting Equation (4.2) into Equation (4.1) resulted in

$$\{\dot{P}\} = [M]^{-1}\{\{R\} - [C]\{P\} - [K]\{q\}\} \tag{4.3}$$

Simultaneous solution of Equations (4.2) and (4.3) was obtained using the Runge-Kutta technique.

All input reference displacements and velocities were defined in function subroutines. The rotating shaker force was also defined in a function-subroutine, F(t). For each spring or damping element with admissible input, one function was required. Thus, the 2-D program (CMW2D) has 11 function subroutines and the 3-D program (CMW3D) has 33 function subroutines. This allowed ground input as a function of time only, at any tire and also at the plow blade or digging chain boom.

In order to simulate adequately the digging chain forces or the cutting action of the vibratory plow, the ground coefficients had to be dependent on the blade or boom location. Two subroutines DIG and PLOW were written to vary the ground parameters for the digging chain and plow, respectively. These subroutines were called after each time step and had to be included inside the integration loop. Therefore, the stiffness and damping matrices were changed, if necessary, for each integration time step. Because of the sudden changes in stiffness and damping coefficients, the step sizes had to be carefully chosen, as will be shown in Chapter V.

The mass of the frame assembly for the 2-D model was chosen to be composed of the distributed frame and an arbitrary number of up-to-30 added masses. Total mass, c.g. location, and inertia about that c.g. were

calculated by the program. For the 3-D program all c.g. locations were read along with the inertia matrices.

Both programs calculated and printed, if requested, the rigid body displacements, velocities, and accelerations. All tire forces, plow or digging chain forces, and cab mount forces were printed. The displacements and velocities of the plow point were also printed by the 2-D program.

Up-to-24 output points may be selected on the frame for the 2-D program. At each point the three frame stress resultants were caculated and printed. Because an auxiliary frame analysis program had to be used with the 3-D model, only the frame loads were found. Eight locations on the frame were selected as the primary load points. These were given in Chapter III. The forces and moments at these points were printed and/or punched on cards so that they could be input to another program. All output quantities were printed in tabular form as a function of time.

As stated earlier, the basic structure of both programs is the same. A sequence of operations for a general solution with either program is given in Table III.

TABLE III

GENERAL SOLUTION SEQUENCE FOR
THE COMPUTER PROGRAMS

Step	Description
1	Read and write the input data
2	Calculate frame mass, c.g. locations, and inertia values
3	Calculate the plow linkage or digging chain geometry
4	Generate the mass matrix
5	Generate the stiffness matrix
6	Find the eigenvalues and eigenvectors and print the natural frequencies and mode shapes
7	Generate the damping matrix
8	Set up the numerical integration loop
9	Evaluate the load vectors
10	Integrate the equations for one time step
11	Modify the stiffness and damping matrices
12	Repeat steps 10-12 until total time has been simulated
13	Print displacements, velocities, and accelerations
14	Evaluate and print tire, cab, plow or chain, and frame forces
15	STOP

CHAPTER V

NUMERICAL RESULTS

Verification of the Programs

The two programs which were developed for this research were checked against each other and also against a third general-purpose program SAPIV. The natural frequencies and mode shapes for models consisting of beam and truss elements were compared with those generated by CMW2D and CMW3D. Six different cases were considered and the results are given in Tables IV and V. Although the mode shapes have both inertia and stiffness coupling, the dominant degree of freedom for each frequency is listed.

A five degree of freedom 2-D model was used for the first case. No plow assembly was included because the SAPIV program could not handle the four-bar linkage. Therefore, the frequencies corresponded to two translations and one rotation for the frame, and one translation and one rotation for the cab. The results for case 1 are given in Table IV.

Case 2 involved a 3-D model of the vehicle frame only. All mass and stiffness data concerning other components were given very small values to isolate the 6 rigid body frequencies of the frame from the total 15 calculated by CMW3D. The dimensions of the front axle were also made small to simulate a single restraint point at the front connecting pin. The SAPIV model consisted of a rigid frame elastically supported at three different points in three directions. Values for case 2 are shown in Table IV.

TABLE IV

COMPARISON OF NATURAL FREQUENCIES FROM SAPIV, CMW2D, AND CMW3D

Case 1			Case 2			Case 3		
SAPIV	CMW2D	Mode	SAPIV	CMW3D	Mode	SAPIV	CMW3D	Mode
2.172	2.175	x	1.568	1.586	y	4.753	4.757	u
2.790	2.792	z	2.250	2.351	θ_z	5.028	4.966	v
3.837	3.841	θ_y	2.690	2.690	x	6.735	6.737	θ_w
6.259	6.268	θ_v	3.182	3.183	z	8.710	8.693	w
7.046	7.051	w	3.253	3.267	θ_x	9.212	9.214	θ_v
			3.804	3.808	θ_y	12.310	12.320	θ_u

TABLE V

COMPARISON OF NATURAL FREQUENCIES FROM CMW2D, CMW3D, AND HAND CALCULATIONS

	Case 4			Case 5			Case 6	
Hand	CMW2D / CMW3D	Mode	CMW2D	CMW3D	Mode	CMW2D	CMW3D	Mode
8.321	8.346*	ψ	2.129	2.162	x	1.650	1.655	z
3.509	3.499	η	2.718	2.742	z	3.835	3.836	x
4.414	4.402	α	3.890	3.888	θ_v	5.766	5.664	w
5.033	5.016	ψ	5.533	5.472	θ_y	6.510	6.479	θ_v
			7.777	7.765	w	8.903	8.751	θ_y
			8.321	8.321	ψ			

*Frequency from CMW2D.

For case 3 the six degrees of freedom for the cab were isolated. Very small mass values and very large stiffness values were used for the other components. A frame elastically supported at four points in three directions was modeled with SAPIV. Frequencies for case 3 are presented in Table IV.

The natural frequencies associated with the plow assembly and the front axle rotation were calculated by hand. Each system was modeled with one degree of freedom and then a frequency equation was easily obtained. Appendix G contains a complete derivation for each of the three equations associated with degrees of freedom ψ, α, and η. These coordinates were isolated in the programs CMW2D and CMW3D by proper choice of the mass and stiffness coefficients of the other components. The hand-calculated values were compared with those generated by CMW2D and CMW3D in case 4, which appears in Table V.

For case 5 a comparison of the frequencies from CMW2D and CMW3D was made. The 2-D model did not allow translation in the X-direction between the cab and frame. Therefore, very high stiffness coefficients were used in the 3-D program to model the same behavior for this case. The frequencies associated with the X-Z plane for the 3-D model and those from the 2-D program are given under case 5 in Table V. Because the model used in CMW3D was symmetric with respect to the X-Z plane, these frequencies were uncoupled from those in the Y-Z plane.

Both programs included the plow and digging chain attachments which have slightly different mass and stiffness matrices. Case 5 involved the plow assembly and case 6 was chosen for the digging chain. The mode order changed between cases 5 and 6, because not only were the attachments

different but also the vehicle models were changed. The results for case 6 are shown in Table V.

After checking the frequencies from CMW2D and CMW3D against each other, hand calculations, and SAPIV, the mass and stiffness matrices were assumed to be correct. Because a linear formulation was made in this development, the stiffness and damping matrices were of the same form. Thus, by setting the stiffness and damping coefficients equal and printing both matrices, the damping matrix was checked.

The time-dependent load matrices were also printed and checked for the two programs. The equations of motion were then integrated for a short time period and the displacements, velocities, and accelerations compared from the two programs. All three quantities matched very well as did the plow, digging chain, and tire forces.

Although these few studies did not completely verify the computer solutions, the results were reassuring and were judged to be sufficient for a continuation into the next phase of the research.

Input data, which corresponded to the Ditchwitch model R-100 trencher, were set up for both programs. The natural frequencies were found to lie below the operating shaker force of 18.33 cps. Therefore, a time step of $\Delta T = .005$ was tried for the first integration run. This proved to be unsatisfactory and additional runs were made until a satisfactory time step of $\Delta T = .0005$ was found for the vibratory plow attachment. Sharp changes in the stiffness and damping coefficients due to the plowing action probably account for the small time step required.

The digging chain was found to require an even smaller time step. Values of $\Delta T = .00025$ and $\Delta T = .0001$ were found to be satisfactory for the center and offset positions, respectively. In addition to the

stiffness and damping coefficients, the forcing function for the digging chain was also displacement-dependent which resulted in sharp changes of its magnitude.

After a suitable time step was found a number of investigations were made. The results presented in this thesis are predicted values only and may or may not represent actual operating conditions. The programs were not compared with experimental values because sufficient field data were not available. Therefore, some of the input parameters had to be assumed based on information available in the literature and known behavior of the system. However, the main purpose of this research was to develop the analysis tool and not to provide quantitative answers. These results do illustrate some of the analysis capabilities and should, at least, qualitatively match the real structure.

Two-Dimensional Studies

The first study was made to determine how the ground coefficients affected the response and what range of values should be used. A rotating shaker force of 26,530 (lbs), which matches that of the real machine, was used. The amplitude of oscillation for the actual plow is approximately one-half inch peak to peak. Therefore, the ground coefficients were varied until this amplitude was reached.

After a proper range of values was found, a sensitivity study was made for the ground stiffness and damping coefficients K_5 and C_5, respectively. For a damping factor of C_5 = 300 (lb-sec/in.), the stiffness values were varied from 20,000 to 60,000 (lb/in.) and the average displacement and peak plow force were calculated over the first 0.5 seconds of simulation. Steady operating conditions were reached after

approximately 0.2 seconds. The displacement changed only 0.2 percent around a 0.466 (in.) mean value and the force changed only 0.25 percent around an 8,141 (lb) mean.

A value for K_5 was chosen to be 40,000. The ground damping was then varied from 100 to 500. Figure 9 shows a 4.7 percent change in the amplitude. Figure 10 shows a 124 percent change in peak cutting force and a 135 percent change in backing force. The backing force is the resultant plow force when the blade is traveling backward. The percent change was calculated based on the values of C_5 = 300.

For both cases a stiffness reduction factor of zero was used. This implied that the ground acted in compression only. A reduction factor of 0.25 was chosen for the damping term. The bounce tire stiffness was given a value of 1500 (lb/in.). Based on the results of the first study, the ground coefficients were selected to be K_5 = 40,000 and C_5 = 300. All of these values seemed to be acceptable for the scope of this research and were used in generating the remainder of the results.

The next study was to determine the stress resultants (axial, shear, and bending moment) in the frame due to both the vibratory plow and digging chain. Figure 11 is a plot of the plow force for normal operating conditions. The angle of this resultant plow force is shown in Figure 12. An angle of approximately -71° indicates forward blade motion and that of 109° backward motion. Thus, a positive magnitude in Figure 11 is forward travel and a negative value rearward travel.

As can be expected from the plow force plot, all three stress resultants alternated at the shaker frequency. The resultants were plotted at three different times within one complete cycle. The distribution along the frame extends from 25 inches in front of the front axle to 80 inches

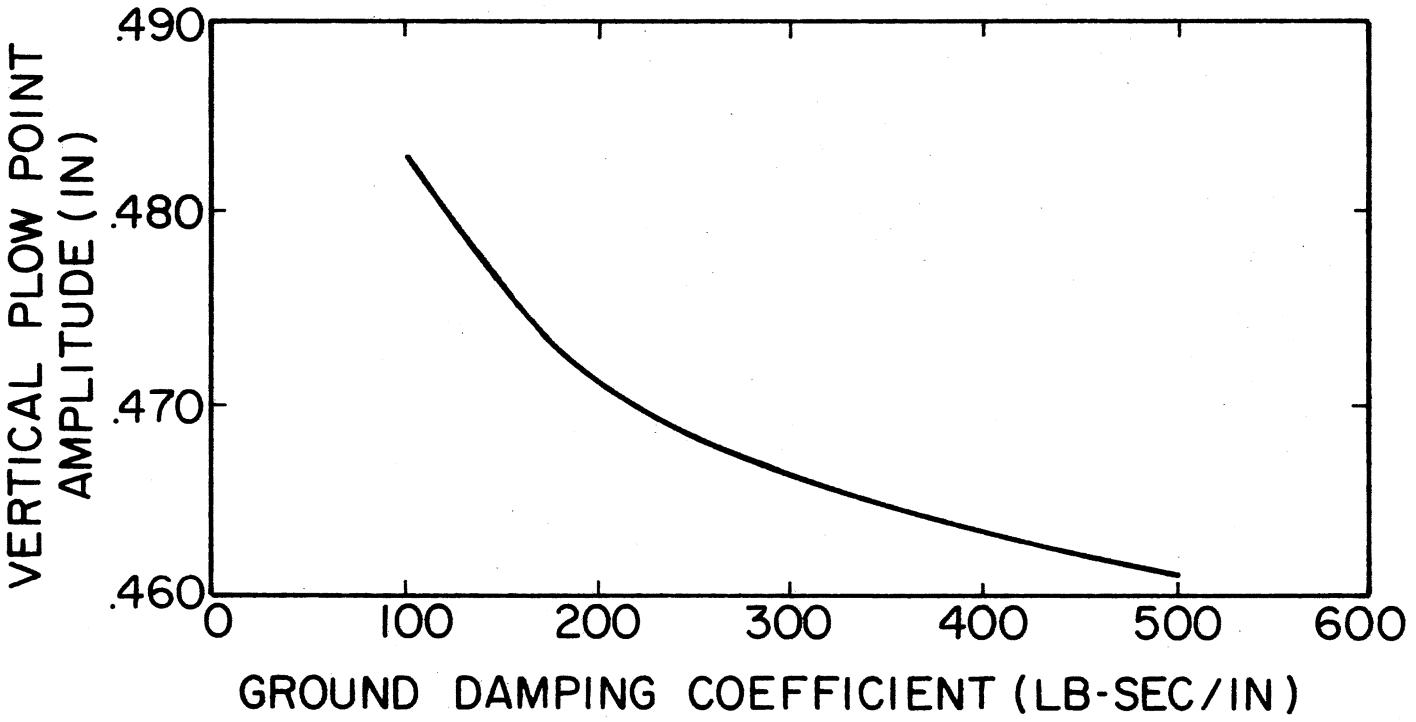

Figure 9. Average Peak-Peak Plow Point Vertical Displacement Amplitude Versus Ground Damping Coefficient for K_5 = 40,000 lb/in.

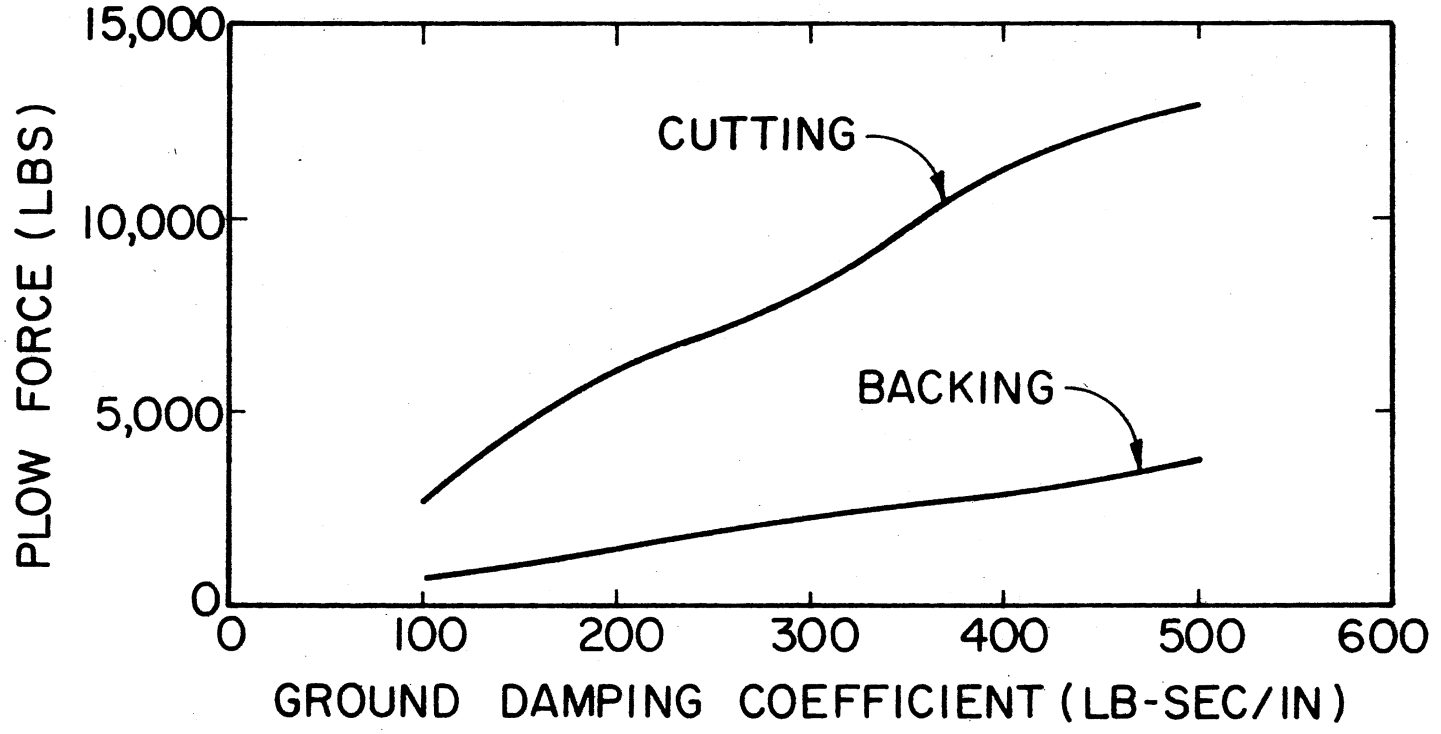

Figure 10. Average Peak Cutting and Backing Plow Force Versus Ground Damping Coefficient for K_5 = 40,000 lb/in.

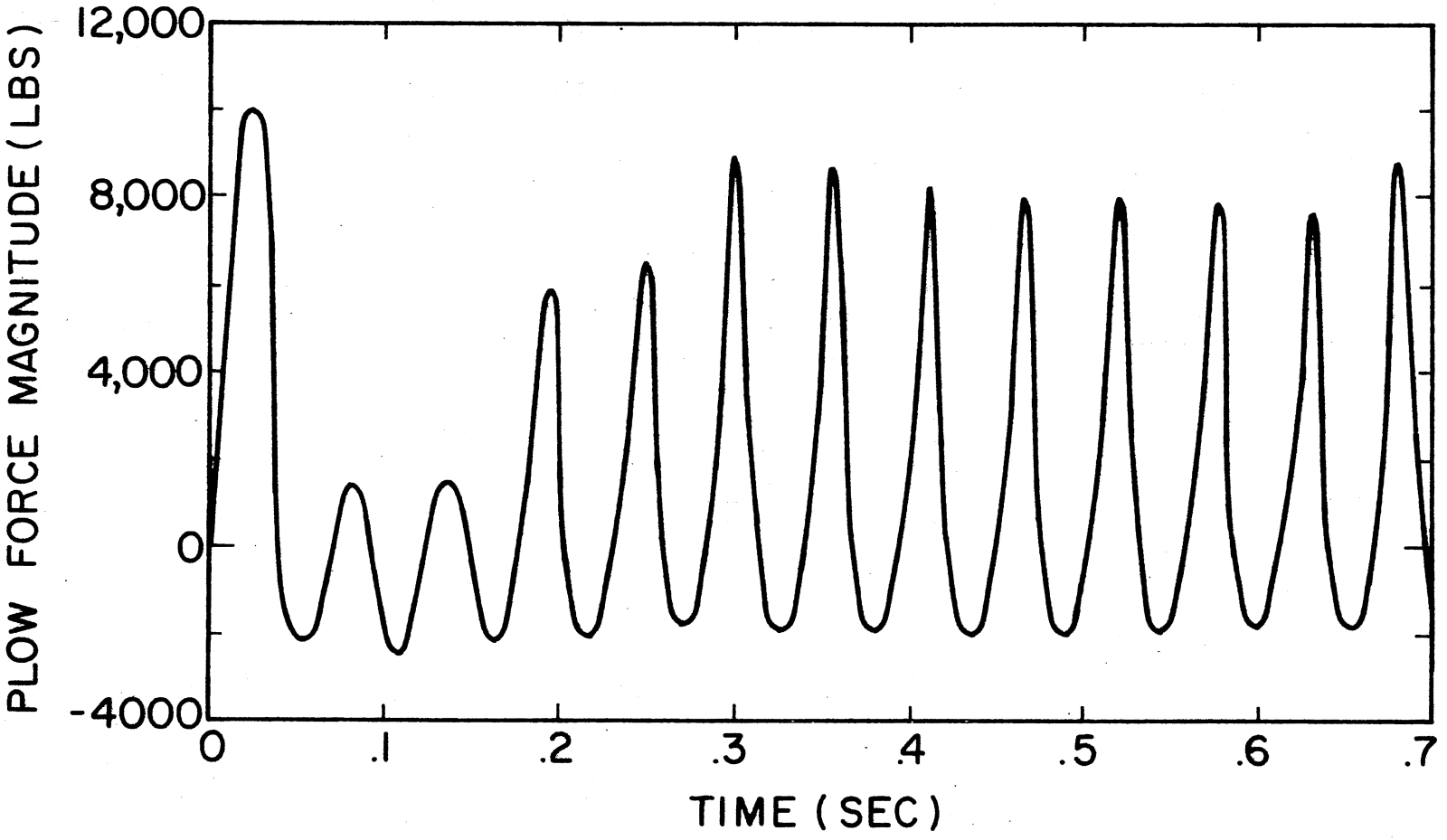

Figure 11. Resultant Plow Force Magnitude

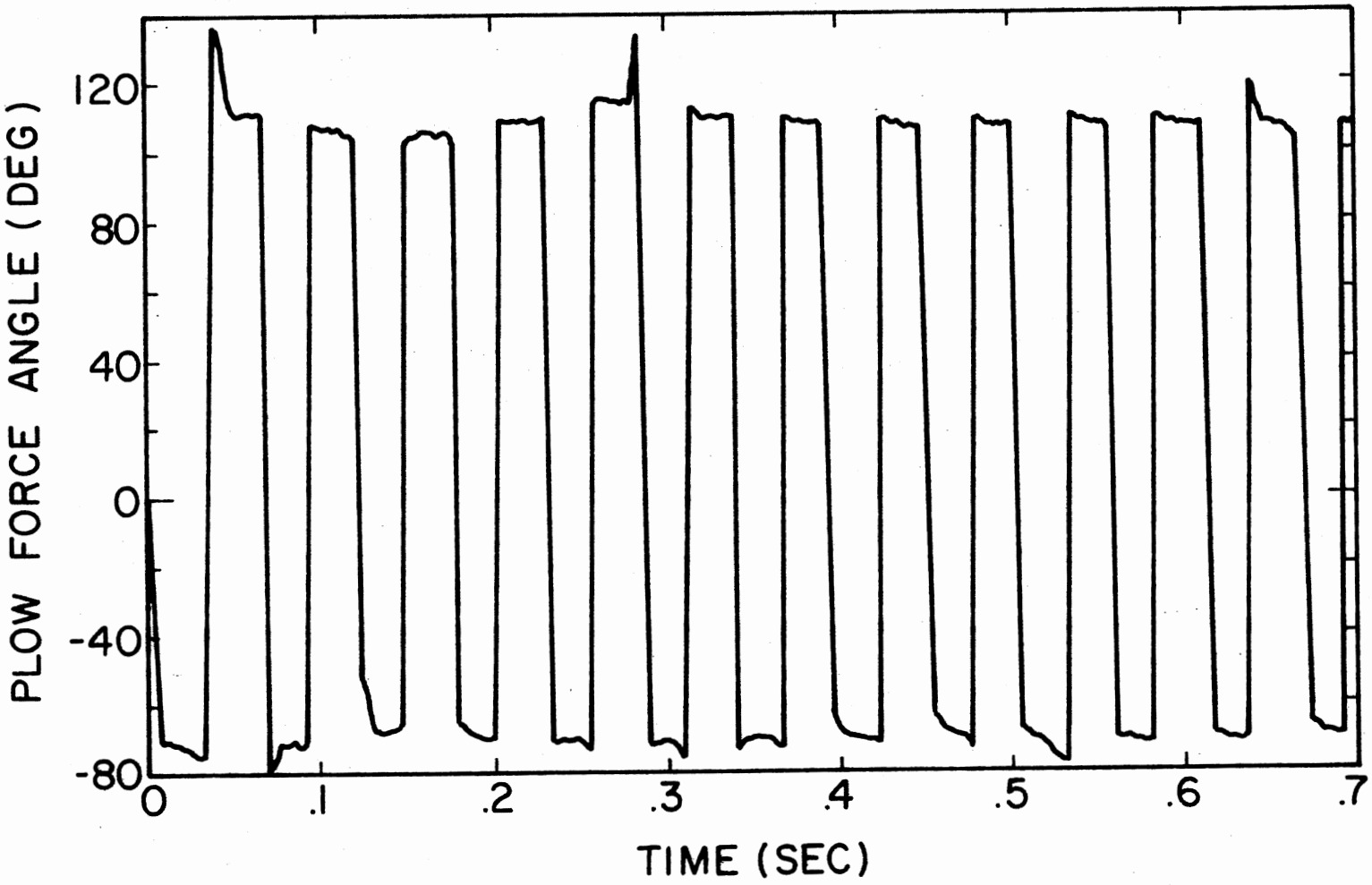

Figure 12. Angle of Plow Force Resultant

behind the front axle. Thus, the origin for all of the plots lies on the neutral axis of the frame tube and directly above the front axle. The axial, shear, and bending stress resultants caused by plowing are given in Figures 13, 14, and 15, respectively. Figure 16 shows the normal stress in the top of the frame tube at a point midway between the axles.

The distribution of the stress resultants for the digging chain was also found. Ground coefficients for the digging chain boom were the same as for the plow. However, the coefficients of the tooth static force and damping value had to be determined. It was assumed that 75 percent of the engine torque went into the digging chain. The linear velocity of the chain was calculated to be 100 (in./sec). Therefore, the two unknown coefficients were chosen so that the peak chain force required all of the available torque. The two reduction factors for the tooth static and damping coefficients were 0.10 and 0.50, respectively. A linear increase in the force was allowed over the first 0.05 seconds to model a starting condition. Figure 17 shows the magnitude of the digging chain force for the first 0.7 second of operation. The four levels of the force depend on the number of teeth digging and the position of the boom with respect to the uncut soil. The above values were used for the rest of the results.

Because of the forcing functions, the vehicle response was quite different for the chain and plow. Although the system natural frequencies were approximately the same, the response was dominated by the forcing frequency for the plow and the rigid body frame frequency for the chain. The stress resultants caused by the digging chain were plotted at three different times. The distribution along the frame for the axial, shear, and bending resultants are given in Figures 18, 19, and 20, respectively.

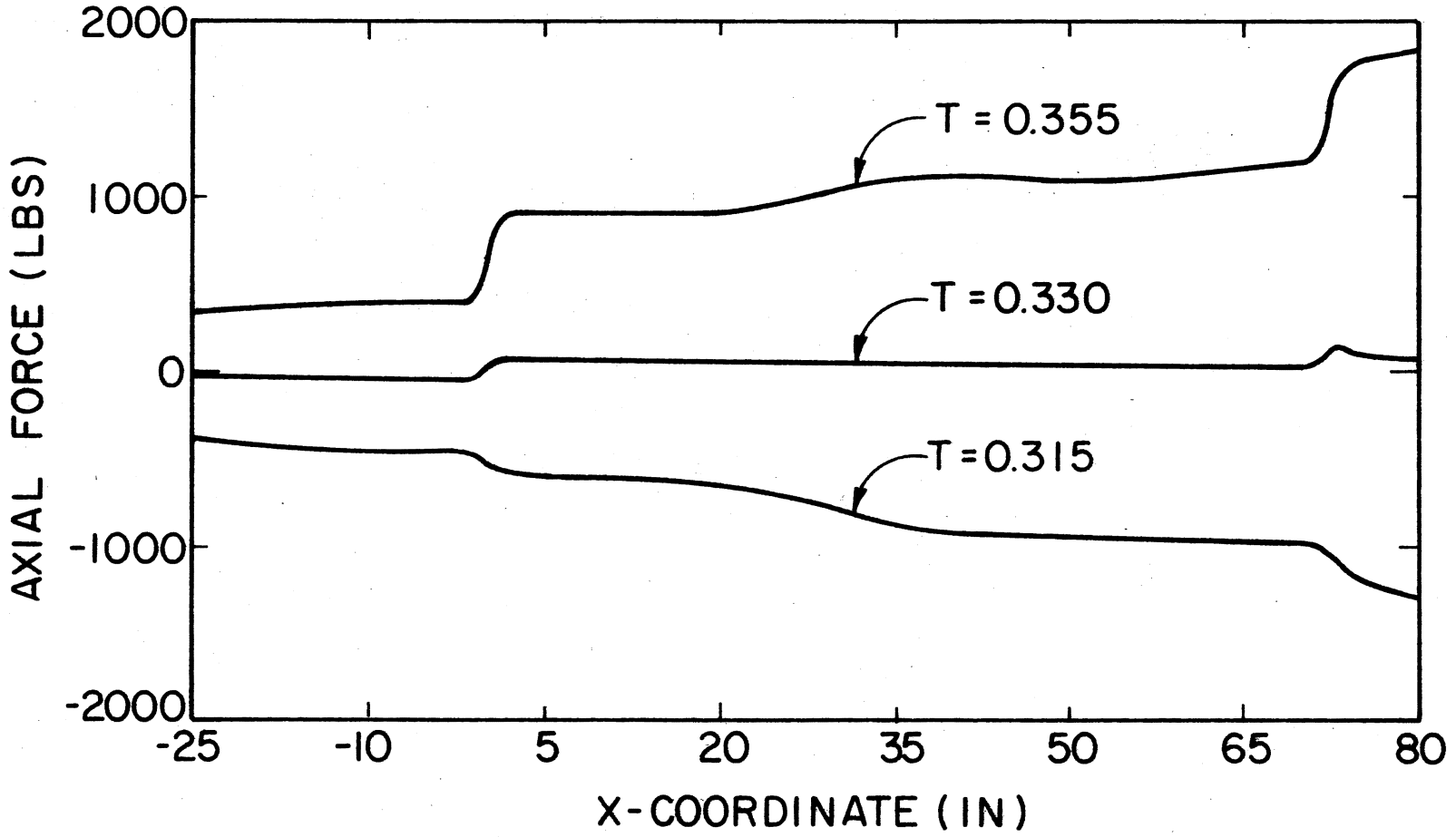

Figure 13. Distribution of the Axial Stress Resultant Along the Frame for Plowing

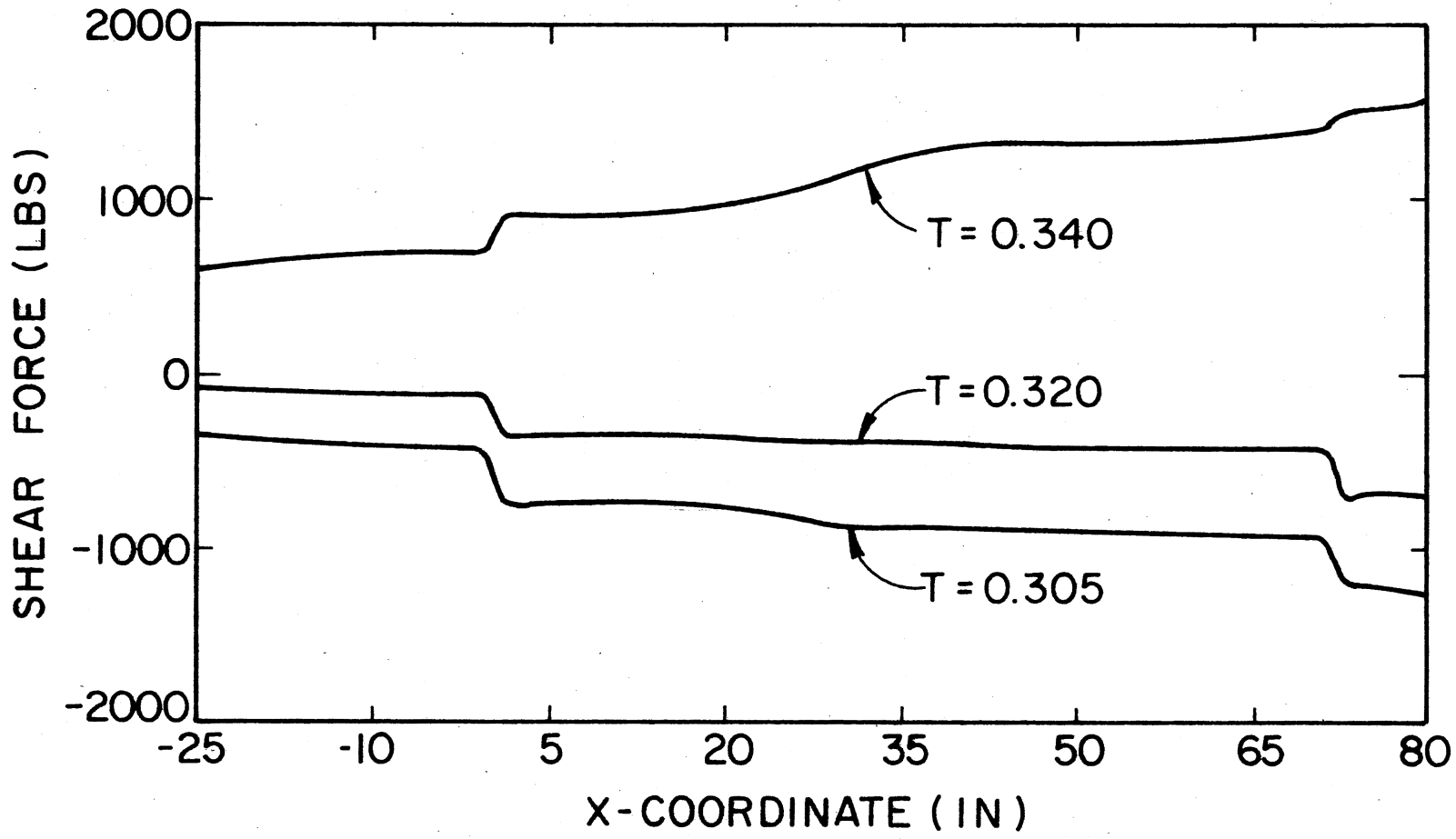

Figure 14. Distribution of the Shear Stress Resultant Along the Frame for Plowing

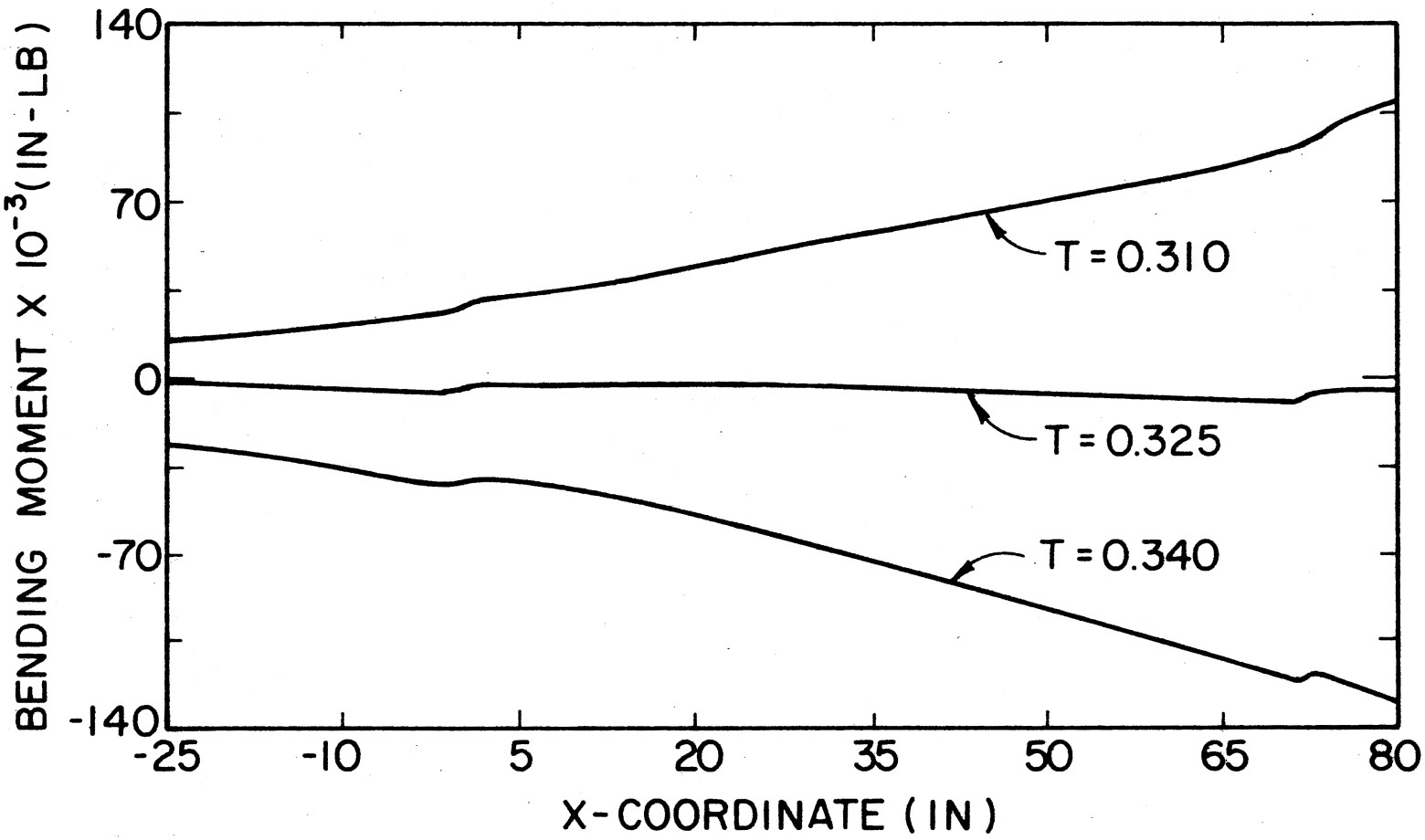

Figure 15. Distribution of the Bending Moment Stress Resultant Along the Frame for Plowing

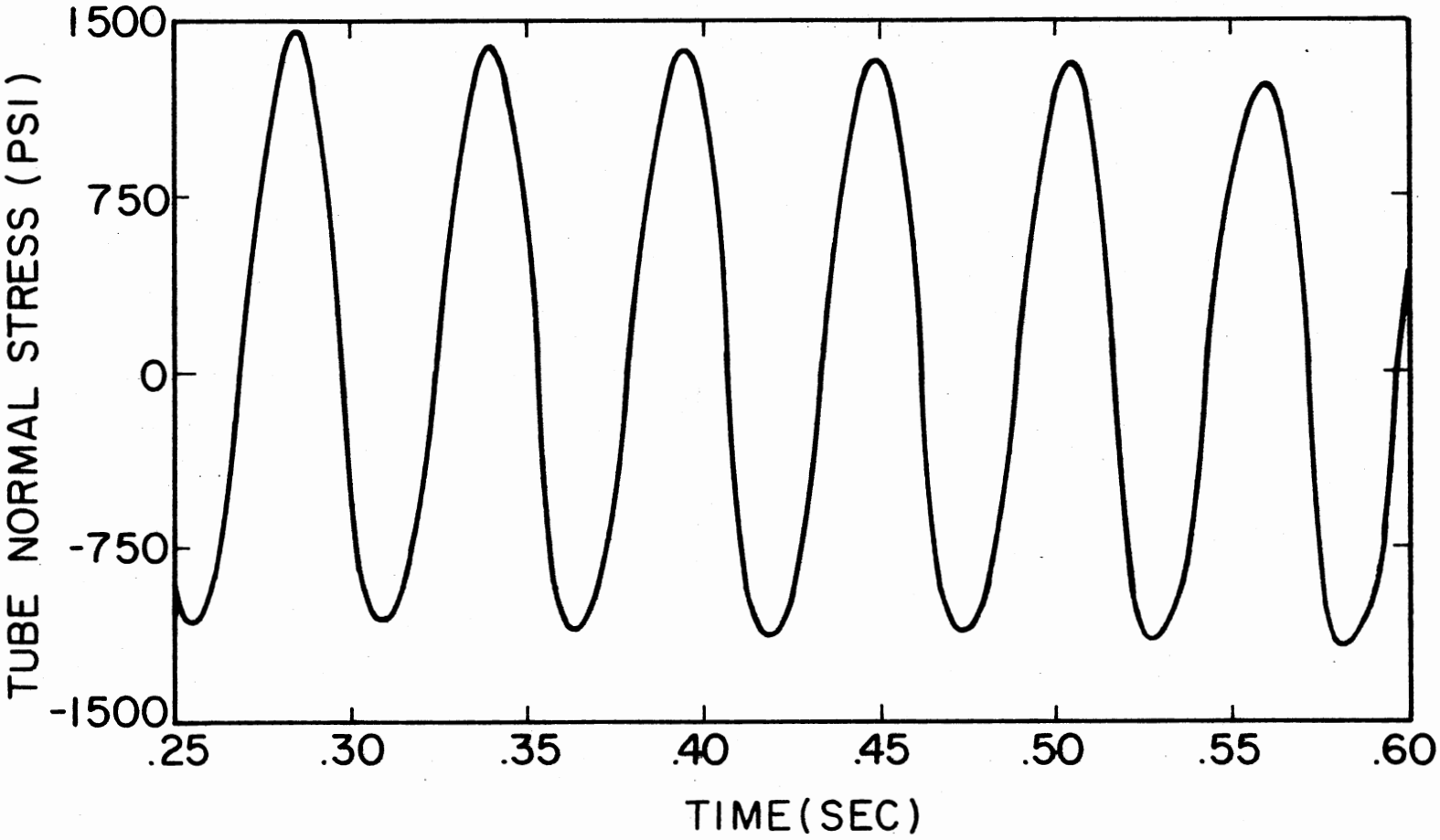

Figure 16. Tube Normal Stress at a Point (X = 36 in.) for Plowing

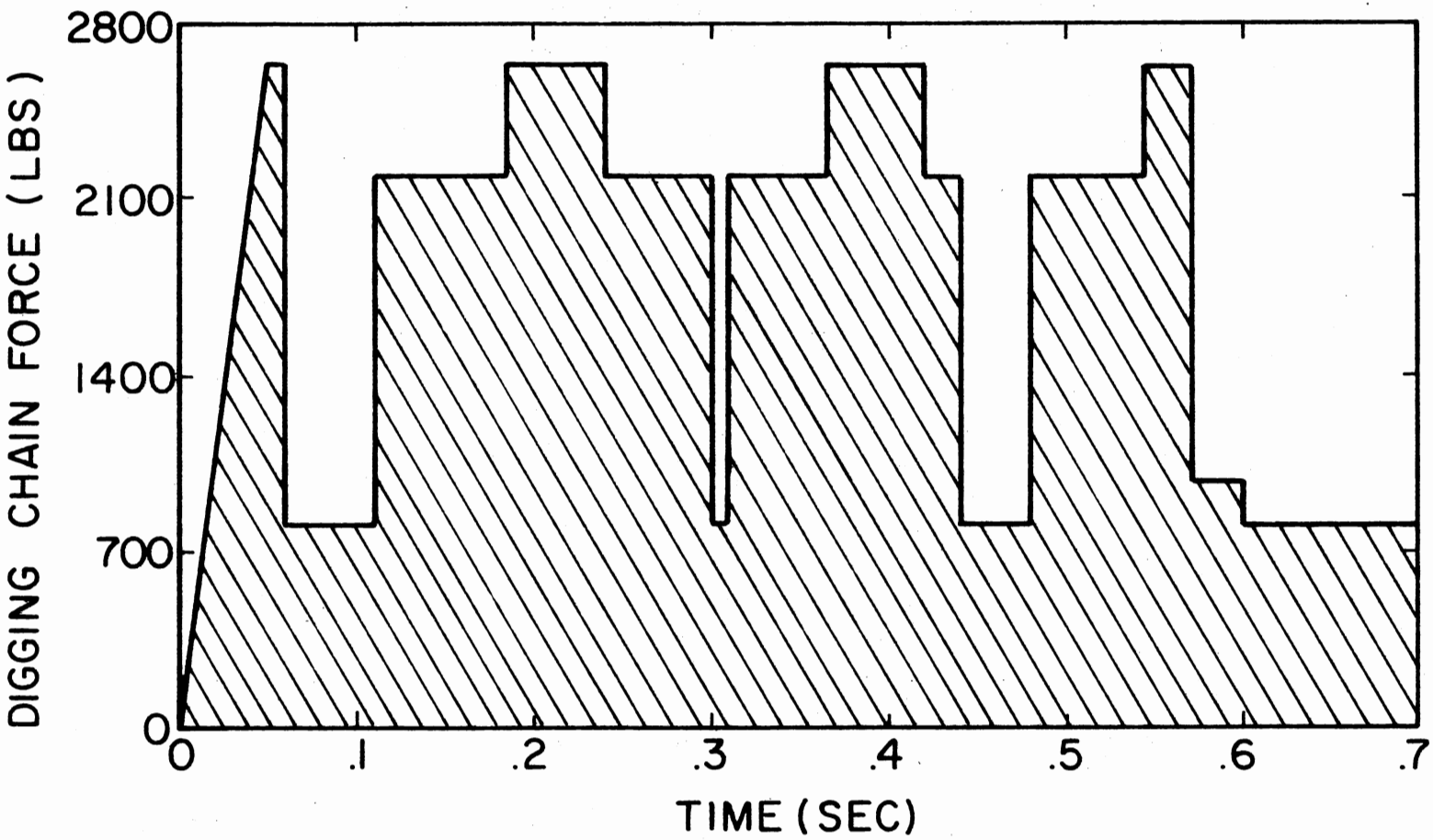

Figure 17. Resultant Digging Chain Force

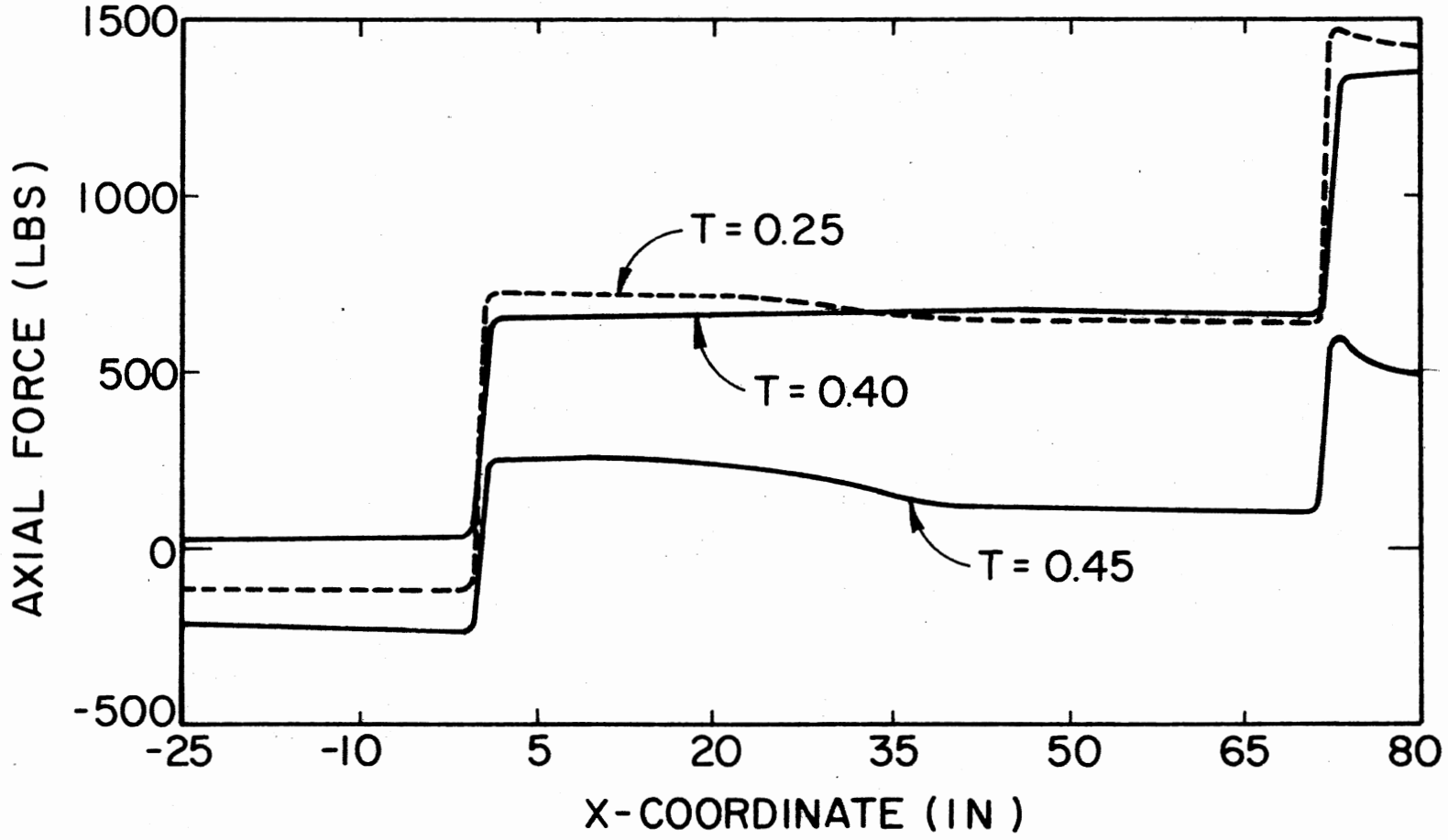

Figure 18. Distribution of the Axial Stress Resultant Along the Frame for Digging

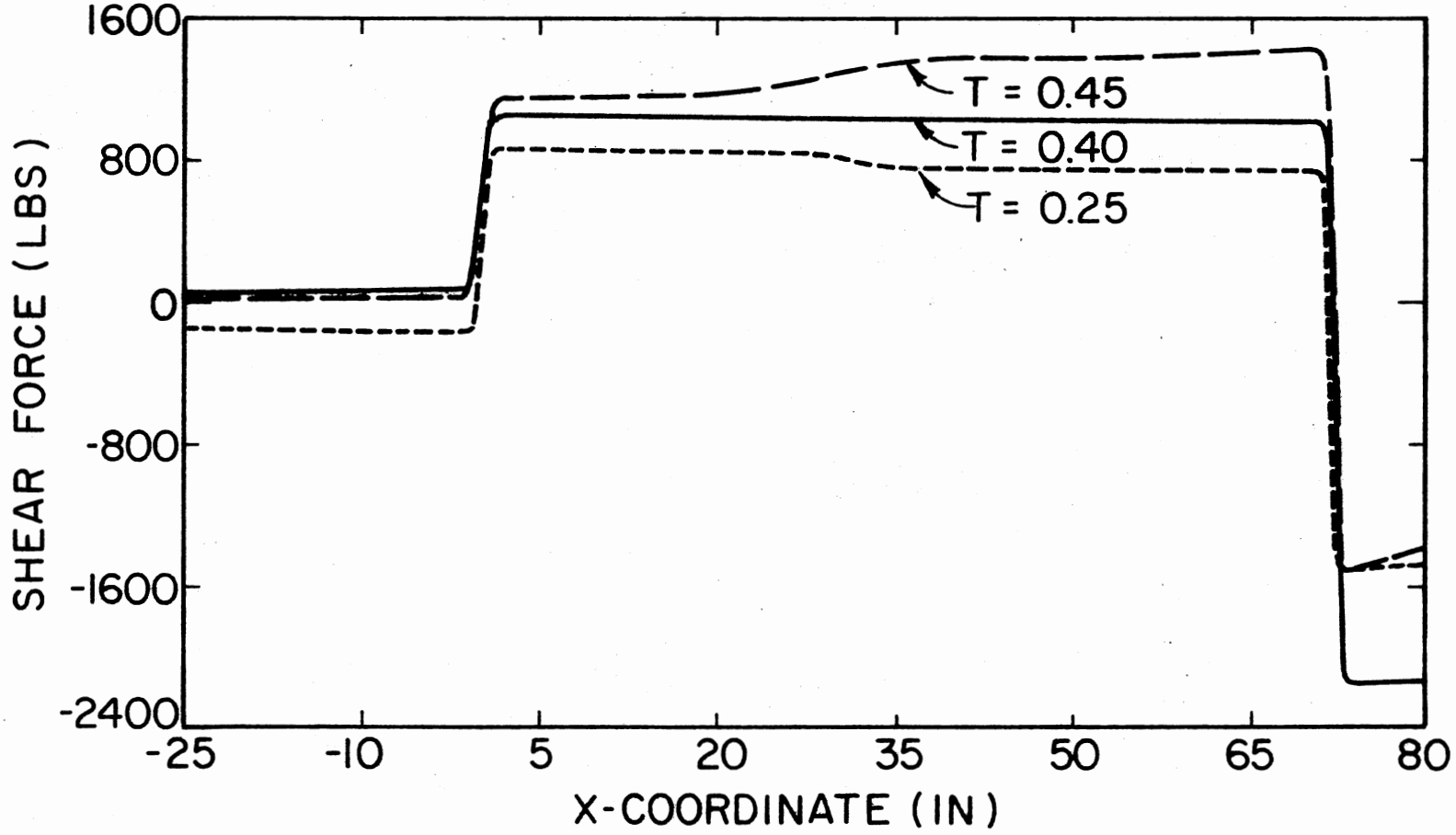

Figure 19. Distribution of the Shear Stress Resultant Along the Frame for Digging

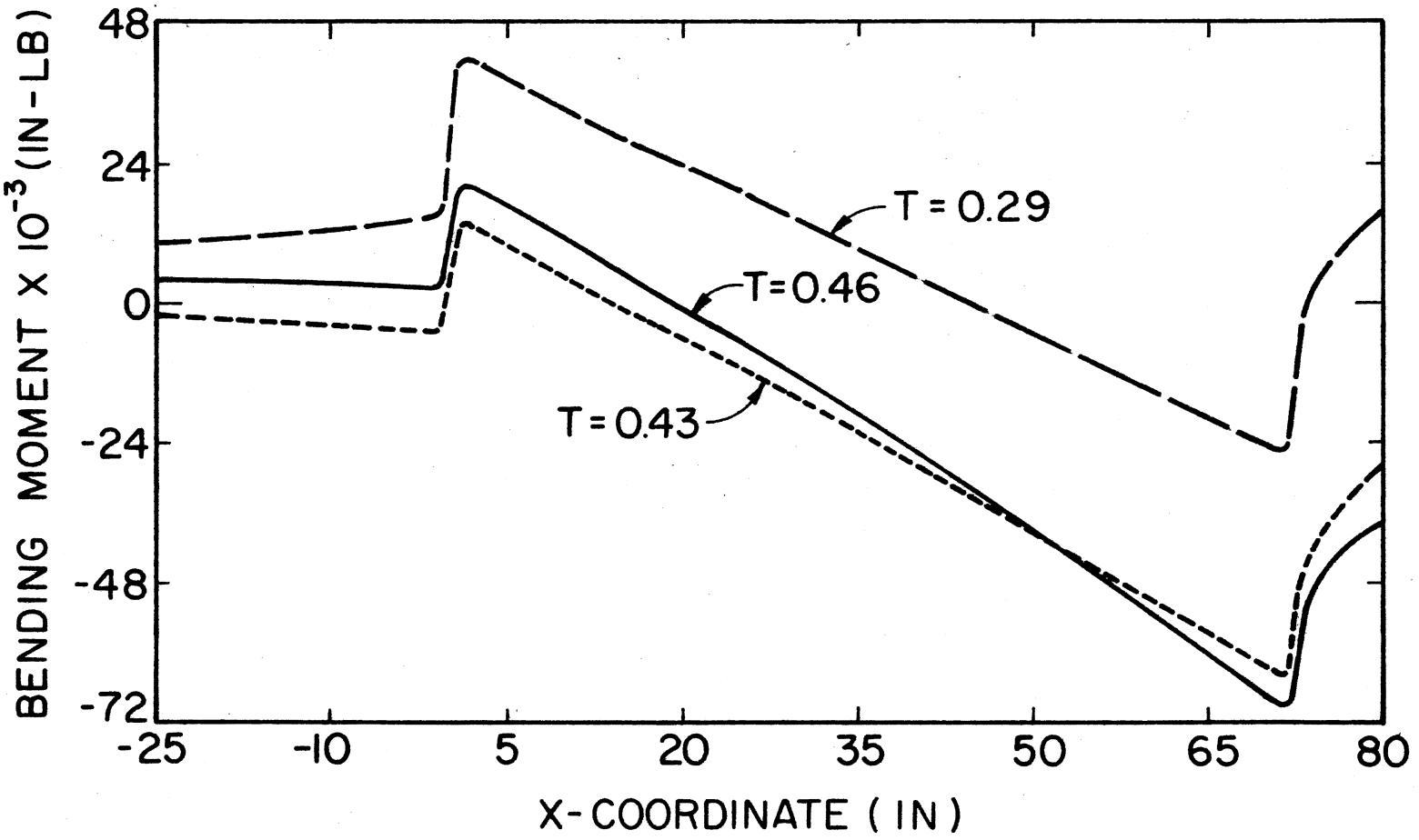

Figure 20. Distribution of the Bending Moment Stress Resultant Along the Frame for Digging

The normal stress in the top of the frame tube at a point midway between the axles is shown in Figure 21. Unlike the plow, the digging chain produced sharp changes in the frame stress because of sudden changes in the total chain force.

Three-Dimensional Studies

The previous studies of the plow and digging chain utilized the 2-D model. It was convenient because the entire analysis was written into the program. However, when offset plowing occurs or a digging chain is attached off-center, the 3-D model must be used. CMW3D generates the frame loads which must be applied to the frame modeled with a separate structural analysis program. Because time and money did not permit a complete analysis for each case studied, only the frame loads themselves from CMW3D were compared. The offset plowing case was set up on SAPIV to illustrate the complete analysis procedure.

The digging chain was first considered to be attached at the center and then at 35 inches to the right or in the positive Y-direction. In general, the forces and moments which act in the X-Z plane change very little for the offset. An example may be seen in Figure 22 where F_x represents the force in the X-direction at the front connecting pin. Naturally, side forces and out-of-plane moments were produced by the offset. These forces and moments had the same general shape as those in the X-Z plane but only half the magnitude. This can be illustrated by F_y in Figure 22. For the offset chain the pitch and roll displacements of the frame were almost the same magnitude while that of the yaw displacement was five to eight times less.

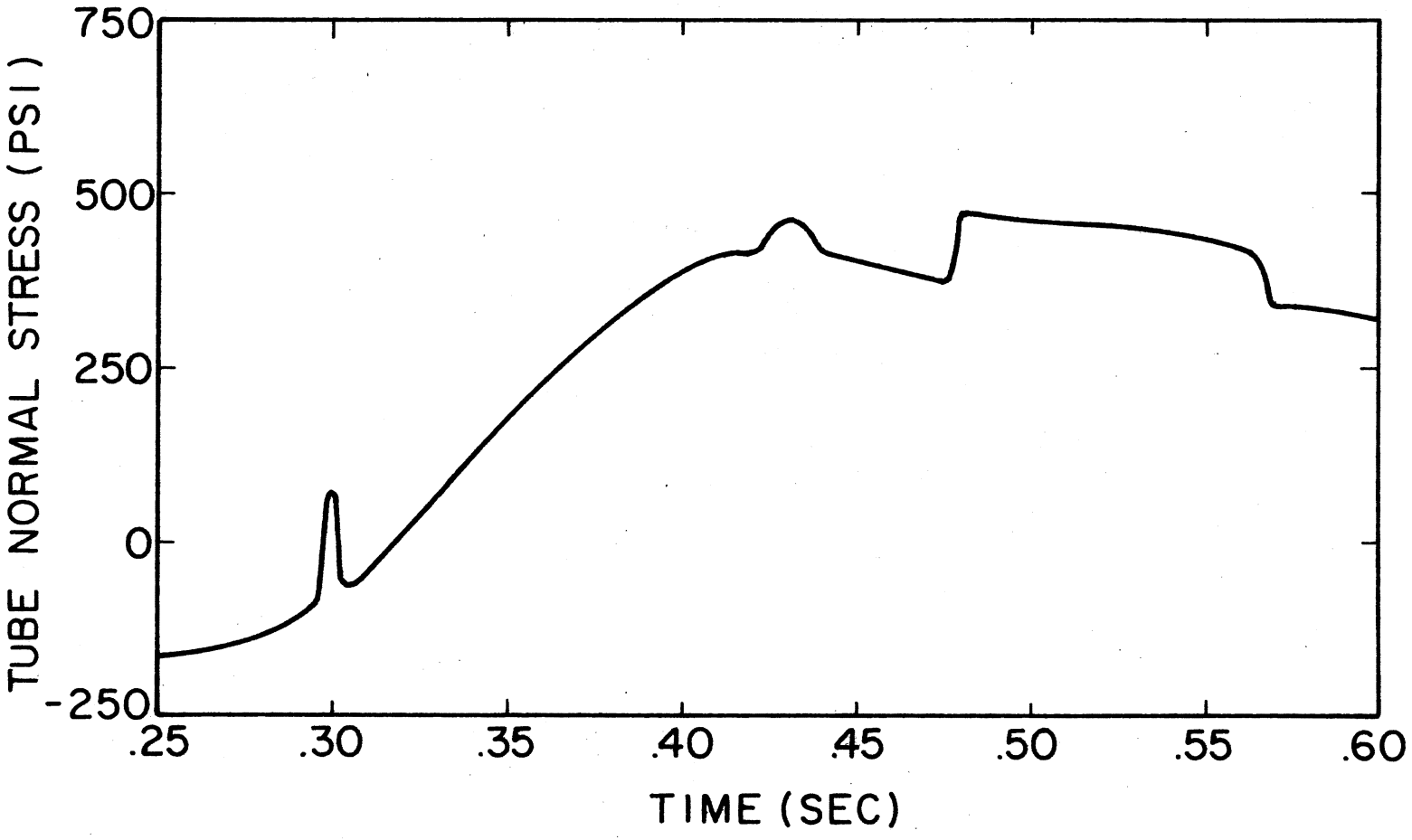

Figure 21. Tube Normal Stress at a Point (X = 36 in.) for Digging

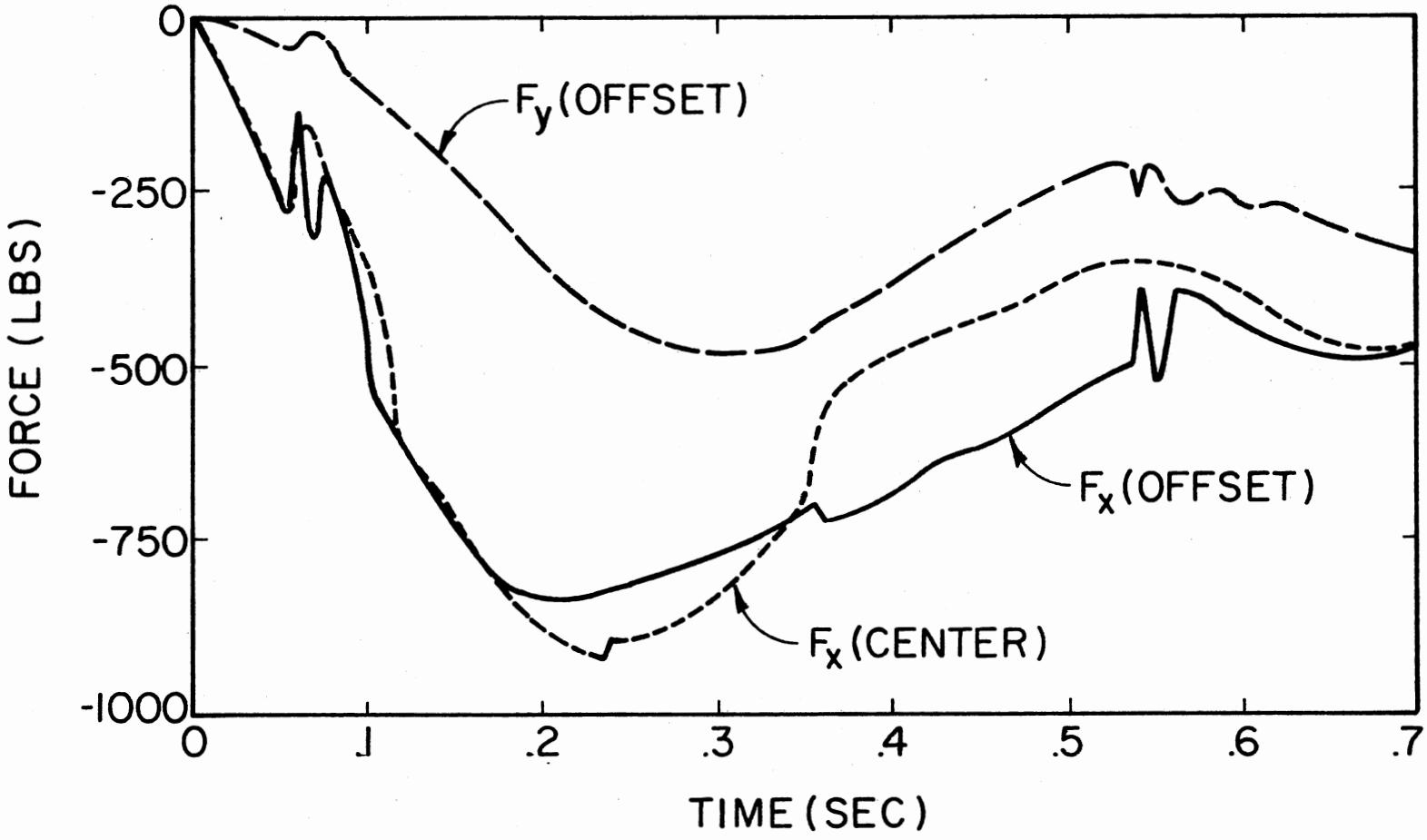

Figure 22. Front Pin Connecting Forces for Both Center and Offset Digging Chain

The main difference between the center and offset chain occurred in the vertical rear axle pin connecting force and the force in the leveling cylinder. For the center-mounted chain the vertical force at the pin is shown as F_z in Figure 23. The leveling cylinder had no force because no rolling forces or moments existed. However, when the chain was moved to the offset position, the vertical force was then input to the frame through the leveling cylinder and the pin-connecting force was greatly reduced. The cylinder force for the offset case is shown as F_c in Figure 23 and the vertical pin force is F_z. Thus, for the offset condition the right side of the frame was much more heavily loaded than was the left.

The final case to be studied was straight and offset plowing. For all runs except offset plowing the wheels remained at zero steer. However, for the offset case both the front and rear wheels were steered to the right an angle of 22 degrees. The blade angle was set at $\beta = 22°$ and the plow boom angle at $\alpha = -1°$. These angles were chosen because they represent the most offset possible for the existing operating machines.

The displacements produced in the offset mode were the same order of magnitude as the in-plane (X-Z) displacements. For this case the yaw of the vehicle had approximately the same values as the pitch and roll modes. Again, the in-plane forces and moments, in general, did not change significantly between straight and offset plowing. Plots of the forces are very similar to Figure 22 as far as differences between the two runs and were not considered necessary for presentation.

As before, the only frame forces significantly affected by the offset mode were the rear axle vertical pin force and the leveling cylinder force. For the straight case the vertical force simply alternated at the forcing frequency. The force is shown as F_z in Figure 24. In the offset

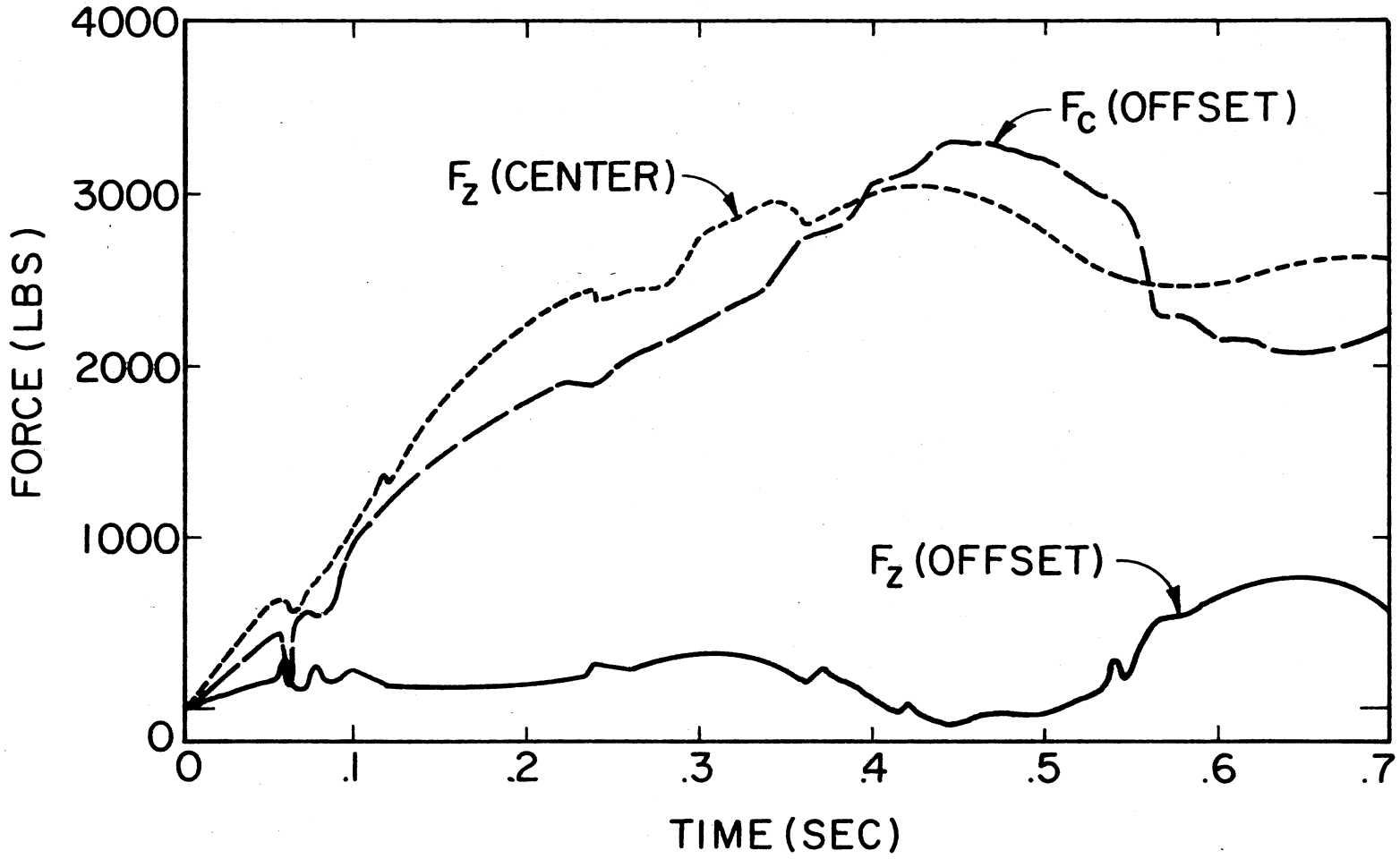

Figure 23. Rear Pin Connecting Force and Leveling Cylinder Force for Both Center and Offset Digging

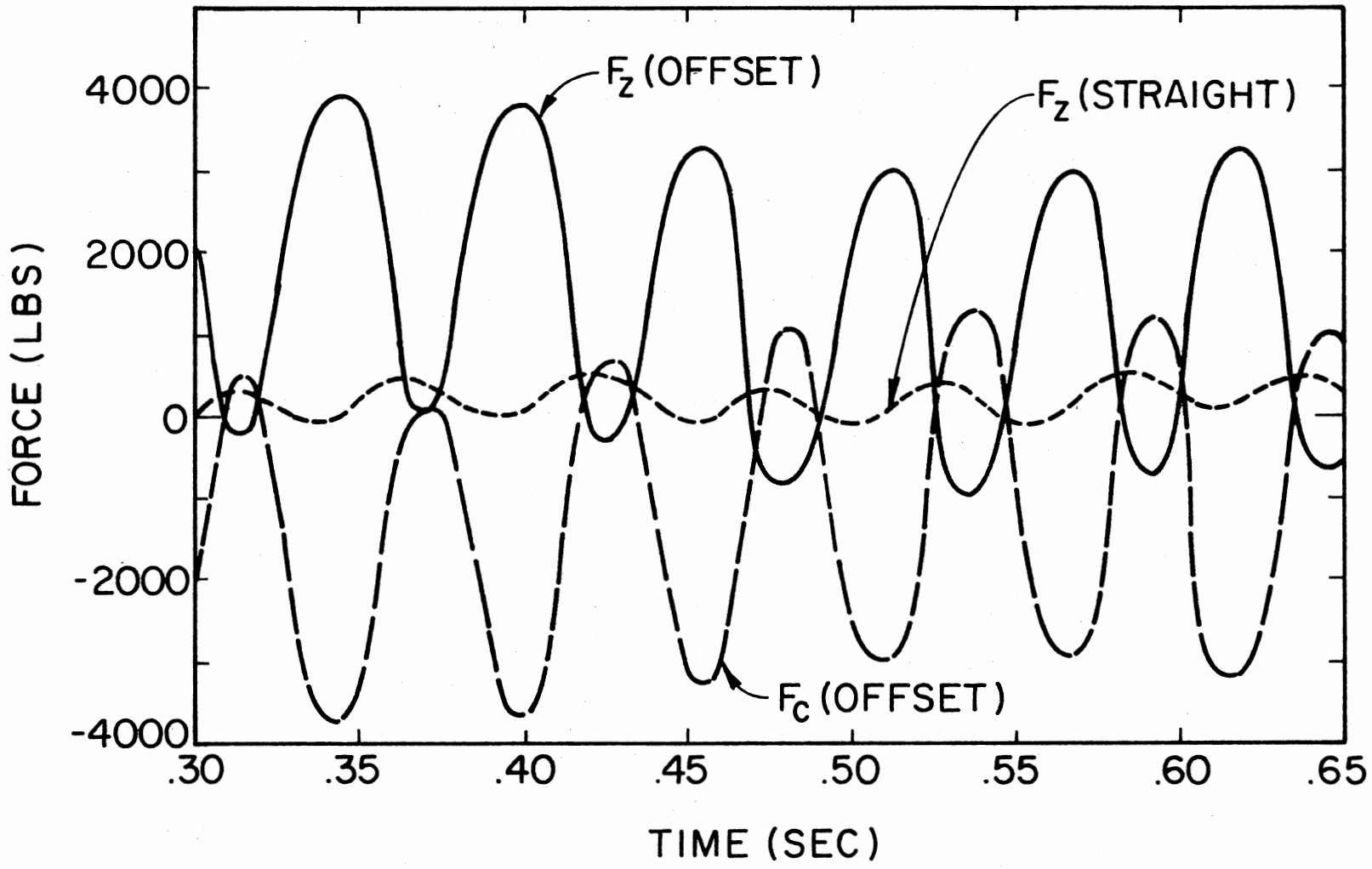

Figure 24. Rear Pin Connecting Force and Leveling Cylinder Force for Both Straight and Offset Plowing

position a moment was generated which had to be reacted by a couple between the connecting pin and the leveling cylinder. The pin and cylinder forces are shown in Figure 24 as F_z and F_c, respectively. By comparison, the vertical pin forced caused by offsetting was approximately seven times that for straight plowing.

A model of the frame was set up with SAPIV. The model consisted of 51 nodes and 61 3-D beam elements. All dimensions and section properties were taken from the R-100 frame layout. Reference (21) contains a detailed description of the frame model. The rear end of the frame was fixed, thereby producing two cantilever beams which were connected by cross members. This support system was incorrect but was deemed adequate for the results of this research.

Frame loads were output from CMW3D in the form of punched cards and then were input to the frame model. In order to reduce computer costs and set-up time, the frame loads resulting from the operator cab were not included in the SAPIV model. However, these forces and moments were small compared to the other frame loads and thus omitting them probably induced only small errors.

A mode superposition technique was used for the dynamic solution of the frame model. This was chosen over a direct integration method because the cost was greatly reduced by considering only a few of the lower modes. However, this eliminates the high frequency response and may cause significant errors in the results for some models. For this case only the first ten modes were considered.

The axial vibrations of the frame were high frequency and were not obtained with the ten-term approximation. However, based on the previous results the frame loading was primarily due to bending. Because the

bending modes were dominated by the lower frequencies, the ten terms were sufficient for this approximate analysis. Figure 25 illustrates the different bending moment distribution down the left and right sides of the frame due to offset plowing.

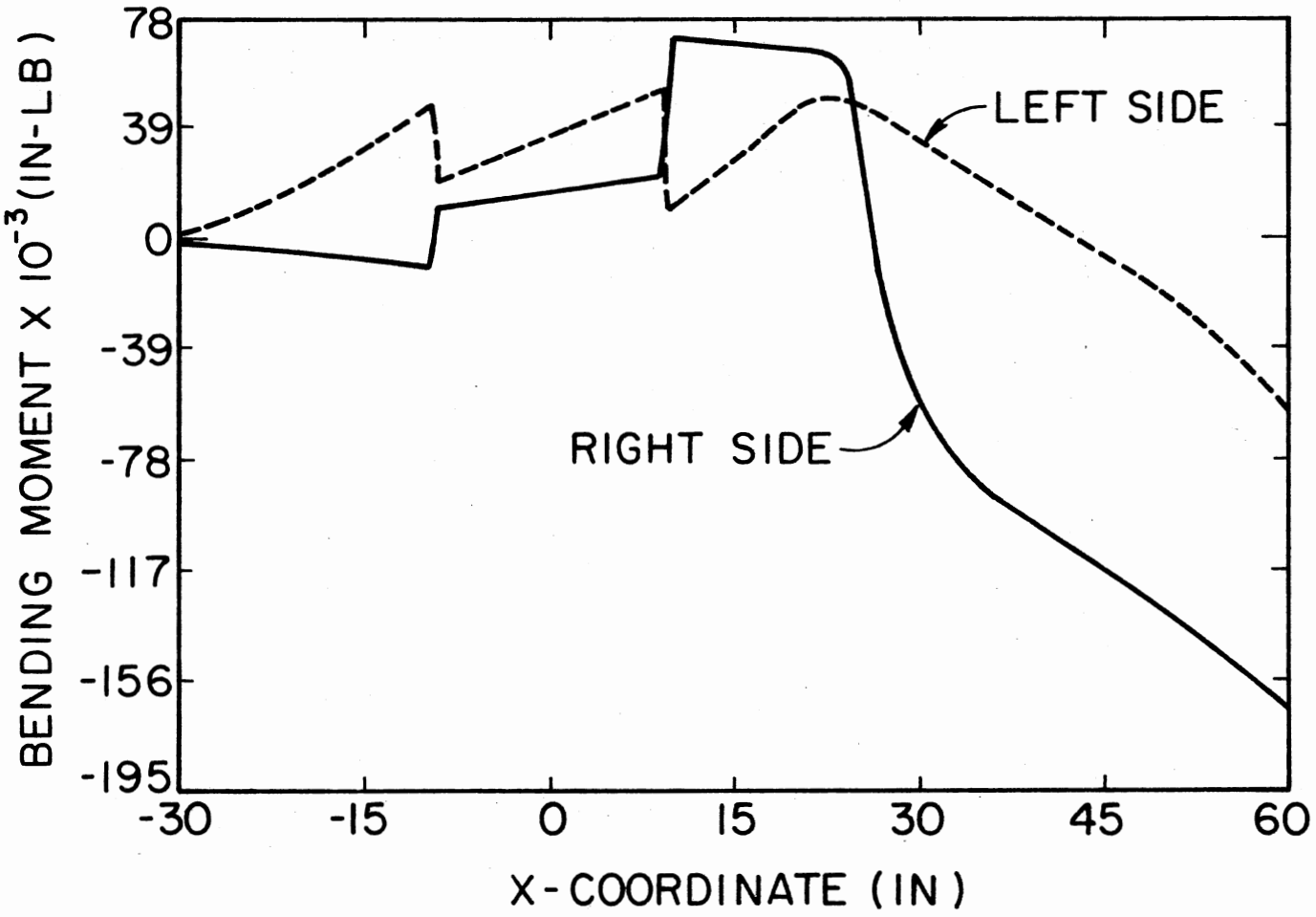

Figure 25. Bending Moment Stress Resultant Along the Left and Right Sides of the Frame for Offset Plowing

CHAPTER VI

SUMMARY, CONCLUSIONS, AND RECOMMENDATIONS

This research has been conducted to develop a dynamic analysis technique which can be used primarily in the frame design of vibratory plow and trenching machines. The analysis programs resulting from this work calculate the rigid body displacements, velocities and accelerations for the frame, cab, and plow assemblies. All tire, plow, and digging chain forces are evaluated and applied to the frame. The acceleration of internal components which are rigidly attached to the frame are also calculated along with their corresponding frame loads. Finally, the axial, shear, and bending frame stress resultants are evaluated at points which are arbitrarily located on the frame.

The problem was divided into two parts: (1) a 2-D model with 6 degrees of freedom, and (2) a 3-D model with 15 degrees of freedom. Both models included the plow and digging chain attachments. The equations of motion were derived in matrix form using the Lagrangian technique.

Separate computer programs were written for the two parts. Each program can perform a free and/or forced vibration analysis. The forced response was obtained by numerical integration of the equations of motion. Allowable forcing functions were: (1) the rotating shaker force, (2) the digging chain force, and (3) ground displacements and velocities at the tires, plow blade, and digging boom. The programs were verified by comparing their natural frequencies and mode shapes with those obtained from

SAPIV and single degree of freedom models. The two programs were compared with each other for the forced response. After the programs were checked out, the following tasks were performed.

1. A study was made to determine an acceptable range of ground coefficient values.

2. The distribution along the frame of the three frame stress resultants was found due to both the vibratory plow and digging chain.

3. The frame loads were compared for the digging chain attached in the center position and then offset to the right 35 inches.

4. The frame loads were compared for the vibratory plow in the straight position and then with the blade offset at 22 degrees.

5. An analysis for offset plowing was performed using SAPIV with a beam element model of the machine frame.

The observations and conclusions made from this study are listed below.

1. The method of anlaysis (and the associated computer programs) developed to analyze the dynamic response and frame stresses of the vehicle provided results that were physically reasonable for the cases studied.

2. For the developed models the ground stiffness coefficient had very little effect on the plow point displacement amplitude or the resultant plow force.

3. The ground damping coefficient had a significant effect on the plow amplitude and force, thus suggesting that the plowing action is mainly velocity-dependent.

4. All three frame stress resultants alternated at the shaker frequency about a near zero mean with the plow assembly. Therefore, the

acceleration for each generalized coordinate had the same frequency as the shaker.

5. Steady operating conditions were obtained after approximately 0.3 seconds of simulation time for both the vibratory plow and digging chain.

6. At least 90 percent of the maximum normal stress in the top and bottom of the frame tube resulted from bending for the vibratory plow.

7. The frame stress resultants caused by the digging chain tended to be dominated by the lower order rigid body modes of the vehicle.

8. The average maximum normal stress in the frame caused by the plow was approximately twice that of the digging chain and at a much higher frequency.

9. Forces and moments, in general, which lie in the X-Z plane did not change significantly when the digging chain was attached off-center or the plow blade was offset.

10. With the digging chain off-center the vertical load at the rear axle was input almost entirely at the leveling cylinder, therefore heavily loading the right side of the frame.

11. Offset plowing reduced the net vertical load applied at the rear axle, but created an external moment which had to be reacted by a couple through the rear axle connecting pin and the leveling cylinder.

Recommendations for further study concerning this research are given as follows.

1. The natural frequencies and mode shpaes of the vehicle should be measured experimentally to determine if damping should be included in the free vibration analysis.

2. Experimental studies should be made to correlate the results from the computer programs with those measured during actual operating conditions. This would allow the programs to be used as a valuable design tool.

3. Parametric investigations should be made of vehicle, plow linkage, and digging chain geometry to determine what effect each has on the dynamic response of the overall system.

4. For this research no degree of freedom was allowed between the cab and frame in the X-direction for the 2-D model. It should be determined if a significant change occurs in the results by including this freedom.

5. All mass for the plow assembly was assumed to be located on link ℓ_2 of the linkage. It should be determined if distributing the total mass among all three moving links has a significant effect on the response.

6. Plotting capabilities could be added to the programs in order to reduce the time and effort required to analyze the tabulated output.

7. The 3-D program developed during this research could be extended to handle an arbitrary number of masses rigidly attached to the frame. By including all major masses and calculating their frame forces, the frame stresses could be found at any particular time using a static analysis. This would eliminate the costly integration of a frame model having many degrees of freedom.

8. The plow point displacements and velocities can be easily obtained from either program. Therefore, the analysis could be extended to calculate the power requirements for driving the vibratory plow.

9. A study should be made to determine the effects of ground displacements, tire, and cab-mount characteristics, and vehicle geometry on the operator module response.

10. An investigation should be made to determine the effects of shaker frequency and plow linkage geometry on the critical speed of the machine.

BIBLIOGRAPHY

(1) Miers, Bruce W. "Mechanical System Behavior and Mathematical Simulation." Paper 730444 presented at SAE Earthmoving Industry Conference, Peoria, Illinois, April, 1973.

(2) Boyd, D. E., and D. L. Turney. "Frame Stresses in the R-200 Vibratory Plow for the Straight Ahead Plowing Mode." Final Report. Charles Machine Works, Perry, Oklahoma, March, 1976.

(3) Boyd, D. E., and D. L. Turney. "Development of an Analysis Procedure for Vibratory Plows Including the Off-Set Plowing Mode." Final Report. Charles Machine Works, Perry, Oklahoma, December, 1976.

(4) Hayden, R. W. "Stress Testing of Clark Model 45B Tractor Shovel." Paper 740708 presented at SAE Farm, Construction & Industrial Machinery Meetings, Milwaukee, Wisconsin, September, 1974.

(5) Horvath, J. K. "Structural and System Models." Paper 750135 presented at SAE Automotive Engineering Meetings, Detroit, Michigan, January, 1975.

(6) Borowski, V. J., R. L. Steury, and J. L. Lubkin. "Finite Element Dynamic Analysis of an Automotive Frame." Paper 730506 presented at SAE Automobile Engineering Meeting, Detroit, Michigan, May, 1973.

(7) Marte, J. W., W. A. McClelland, J. R. Lemon, and D. W. Kinsey. "Improved Techniques for Dynamic Analysis of Earthmoving Equipment." Paper 740425 presented at SAE Earthmoving Industry Conference, Peoria, Illinois, April, 1974.

(8) Fanslow, R. J. "200 HP Class Tractor From Concept to Contractor." Paper 740664 presented at SAE Farm, Construction & Industrial Machinery Meetings, Milwaukee, Wisconsin, September, 1974.

(9) Smith, R. E. "Computer Applications for Suspension and Frame Design of Agricultural Equipment." Paper 670723 presented at SAE Farm, Construction & Industrial Machinery Meeting, Milwaukee, Wisconsin, September, 1967.

(10) Pershing, R. L., and R. R. Yoerger. "Simulation of Tractors for Transient Response." Transactions of ASAE, Vol. 12 (1969), pp. 715-719.

(11) Smith, D. W. "Computer Simulation of Tractor Ride for Design Evaluation." Paper 770704 presented at SAE Off-Highway Vehicle Meeting, Milwaukee, Wisconsin, September, 1977.

(12) Larson, D. L., D. W. Smith, and J. B. Liljedahl. "The Dynamics of Three-Dimensional Tractor Motion." Transactions of ASAE, Vol. 19 (1976), pp. 195-200.

(13) Rehkugler, G. E., P. Atherton, and J. E. Kelly. "Simulating the Motion of Two- and Four-Wheel Drive Tractors." Agricultural Engineering, Vol. 59 (1978), pp. 17-19.

(14) Shaw, L. N., W. H. Johnson, and M. Y. Handy. "Analyzing Dynamic Responses of a Semi-Mounted Implement." Transactions of ASAE, Vol. 15 (1972), pp. 1059-1063.

(15) Boyd, R. J., and C. L. Nalazny. "A Model of Vibratory Soil Cutting." Paper 670750 presented at SAE Farm, Construction & Industrial Machinery Meeting, Milwaukee, Wisconsin, September, 1967.

(16) Senator, M. "Vibratory Penetration of Soils." Transactions of ASME, Vol. 89 (1967), pp. 759-769.

(17) Senator, M., and R. E. Warren. "Predicting Penetration Rates of Plows With Combined Vertical and Fore-Aft Vibration and Flexible Blades." Paper 700040, SAE Automotive Engineering Congress, Detroit, Michigan, January, 1970.

(18) Scerbo, L. J., and D. L. Pope. "Bounding Solutions for Performance of Vibratory Plows." Transactions of ASME, Vol. 96 (1974), Serial B, pp. 954-959.

(19) Scerbo, L. J. "Development of a Prototype Orbital Cable Plow." Transactions of ASAE, Vol. 17 (1974), pp. 640-644.

(20) Boyd, D. E., and D. L. Turney. "Development of a Dynamic Analysis Technique for Vehicle Frames of Vibratory Plows and Trenchers--Part 2." Final Report. Charles Machine Works, Perry, Oklahoma, May, 1978.

(21) Boyd, D. E., D. L. Turney, and K. Good. "Deflection Analysis of the Ditchwitch R-100 Frame Subjected to Backhoe Loadings." Final Report. Charles Machine Works, Perry, Oklahoma, March, 1978.

(22) Gill, W. T., and G. E. VandenBerg. "Soil Dynamics in Tillage and Traction." Agricultural Handbook No. 316. U.S. Government Printing Office, Washington, D.C., 1967.

(23) Froberg, Carl-Erik. Introduction to Numerical Analysis. Reading, Massachusetts: Addison-Wesley, 1969.

(24) Greenwood, D. T. Principles of Dynamics. Englewood Cliffs, New Jersey: Prentice-Hall, 1965.

(25) Soni, A. H. Mechanism Synthesis and Analysis. New York: McGraw-Hill, 1974.

(26) Meirovitch, L. Elements of Vibration Analysis. New York: McGraw-Hill, 1975.

APPENDIX A

DERIVATION OF THE DISPLACEMENT VECTOR FOR A PLOW BLADE POINT FOR THE 2-D MODEL

The geometry for the tractor and plow assembly is shown in Figures 1, 2, and 3. The displacement of point 6 was expressed as

$$\Delta_6 = (x + d_6\theta_y)\ell + (z - a_6\theta_y)n \tag{A.1}$$

The displacement of point 9 was written as

$$\Delta_9 = \Delta_6 + \Delta_{9/6}$$

where

$$\Delta_{9/6} = -(\ell_1 \sin\psi')\psi\ell + (\ell_1 \cos\psi')\psi n$$

or

$$\Delta_9 = [x + d_6\theta_y - (\ell_1 \sin\psi')\psi]\ell + [z - a_6\theta_y + (\ell_1 \cos\psi')\psi]n \tag{A.2}$$

A primed angle will denote the equilibrium or starting position.

The ℓ^*-n^*-axis system was fixed to link ℓ_2 with n^* being parallel to ℓ_2 and with the origin at point 9. Thus, any point on the plow blade can be defined with respect to point 9 as

$$\rho_i^* = XP_i\ell^* + ZP_i n^* \tag{A.3}$$

However, the ℓ^*-n^* system was rotated an angle ψ_1' with respect to the ℓ-n axes. Thus, the position vector was transformed into the ℓ-n axis system.

Angle ψ_1' was defined with the four-bar equation as follows.

$$\psi_1' = 2\tan^{-1}\left[\frac{-E - \sqrt{E^2 - 4DF}}{2D}\right] \tag{A.4}$$

where

$$D = LK_4 \cos\theta_2' + \cos\theta_2' + LK_5 - LK_1$$

$$E = -2 \sin\theta_2'$$

$$F = LK_4 \cos\theta_2' - \cos\theta_2' + LK_5 + LK_1$$

$$LK_1 = (d_6 - d_{11})/\ell_1$$

$$LK_4 = (d_6 - d_{11})/\ell_2$$

$$LK_5 = [\ell_3^2 - (d_6 - d_{11})^2 - \ell_1^2 - \ell_2^2]/2\,\ell_1\,\ell_2$$

$$\theta_2' = \pi/2 + \psi'$$

The transformation equations are

$$\ell^* = \cos\psi_1'\,\ell + \sin\psi_1'\,n$$

$$n^* = -\sin\psi_1'\,\ell + \cos\psi_1'\,n \tag{A.5}$$

Equation (A.5) was substituted in Equation (A.3) which yielded

$$\rho_i = (XP_i \cos\psi_1' - ZP_i \sin\psi_1')\ell + (XP_i \sin\psi_1' + ZP_i \cos\psi_1')n \tag{A.6}$$

The displacement vector of the point with respect to point 9 was found from Equation (A.6). Thus,

$$\Delta_{i/9} = -(XP_i \sin\psi_1' + ZP_i \cos\psi_1')\psi_6\,\ell + (ZP_i \cos\psi_1' - ZP_i \sin\psi_1')\psi_6\,n \tag{A.7}$$

where ψ_6 is the rotation of ℓ_2 caused by the generalized coordinates θ_y

and ψ. For small angles the relationship between the input and output link can be written as

$$d\theta_3 = \frac{[-LK_4\theta_2 + \theta_2 - \theta_3]}{[LK_1\theta_3 - \theta_3 + \theta_2]} d\theta_2 \tag{A.8}$$

In terms of the generalized coordinates and the equilibrium angles, Equation (A.8) is

$$\psi_1 = CB\ \psi \tag{A.9}$$

where

$$CB = \frac{(1 - LK_4)(\psi' + 90) - \psi_1'}{LK_1\psi_1' - \psi_1' + (\psi' + 90)}$$

ψ_6 was defined as

$$\psi_6 = CB\ \psi + (CB - 1)\theta_y \tag{A.10}$$

The total displacement of the point was written as

$$\Delta_i = \Delta_9 + \Delta_{i/9} \tag{A.11}$$

Equations (A.2), (A.7), (A.10), and (A.11) were combined to yield

$$\Delta_i = [x + T1_i\psi + T2_i\theta_y]\ell + [z + T3_i\psi + T4_i\theta_y]n \tag{A.12}$$

where

$$T1_i = -[\ell_1 \sin\psi' + (XP_i \sin\psi_1' + ZP_i \cos\psi_1')\ CB]$$

$$T2_i = [d_6 - XP_i(CB - 1)\ \sin\psi_1' - ZP_i(CB - 1)\ \cos\psi_1']$$

$$T3_i = [\ell_1 \cos\psi' + (XP_i \cos\psi_1' - ZP_i \sin\psi_1')\ CB]$$

$$T4_i = -[a_6 - XP_i(CB - 1)\ \cos\psi_1' + ZP_i(CB - 1)\ \sin\psi_1']$$

APPENDIX B

LIFT CYLINDER DISPLACEMENT AND VELOCITY EQUATIONS

The dimensions associated with element 7 are shown in Figure 2. Points 7 and 8 both lie on rigid members which are connected to a common point 6. Only relative displacement between points 7 and 8 is needed; therefore, the displacement vectors were written with respect to point 6.

The displacement of point 8 was expressed as

$$\Delta_8 = -(\ell_5 \sin\psi' - \ell_{13} \cos\psi')\,\psi\ell + (\ell_5 \cos\psi' + \ell_{13} \sin\psi')\,\psi n \tag{B.1}$$

Correspondingly, the displacement of point 7 was written as

$$\Delta_7 = -(d_6 + \ell_4)\theta_y \ell \tag{B.2}$$

Differentiation of Equations (B.1) and (B.2) yielded the velocities which are given as

$$V_8 = -(\ell_5 \sin\psi' - \ell_{13} \cos\psi')\,\dot{\psi}\,\ell + (\ell_5 \cos\psi' + \ell_{13} \sin\psi')\dot{\psi}\,n \tag{B.3}$$

$$V_7 = -(d_6 + \ell_4)\,\dot{\theta}_y \ell \tag{B.4}$$

The angle of the lift cylinder ψ_3 was defined as

$$\psi_3 = \tan^{-1}\left[\frac{d_6 + \ell_4 + \ell_5 \sin\psi' - \ell_{13} \cos\psi'}{\ell_5 \cos\psi' + \ell_{13} \sin\psi'}\right] \tag{B.5}$$

Because the cylinder sets at the angle ψ_3, the displacement and velocity of the spring and damping element are only the components of Equations (B.1) through (B.4) which are parallel to the element. Thus, the displacement and velocity were given by Equations (B.6) and (B.7), respectively.

$$XK_7 = (\Delta X_8 - \Delta X_7) \cos\psi_3 - \Delta Z_8 \sin\psi_3 \tag{B.6}$$

$$VC_7 = (VX_8 - VX_7) \cos\psi_3 - VZ_8 \sin\psi_3 \tag{B.7}$$

APPENDIX C

CALCULATION OF THE FRAME C.G. LOCATION AND INERTIA

A reference point was chosen and the vehicle geometry defined. The coordinate values for each mass was given. A frame attachment point was also defined for each mass. These values were represented as (XIM_i, ZIM_i) and (XIC_i, ZIC_i), respectively. The mass/unit length of the frame was denoted as ρ and the total length as FLT.

$$FLT = FLF + FLR \tag{C.1}$$

where

FLF = distance from the reference point to the front of the frame; and

FLR = distance from the reference point to the rear of the uniform frame section.

Let M_1 be the total mass of the frame and all components except the plow assembly and operator cab. Therefore,

$$M_1 = \sum_{i=1}^{n} CCM_i + FLT \tag{C.2}$$

where CCM_i is the value of the ith mass. The c.g. location was then defined as

$$ZCG = \left(\sum_{i=1}^{n} CCM_i \; ZIM_i + M_3 \; d_{20} \right) / (M_1 + M_3) \tag{C.3}$$

and

$$XCG = [(\sum_{i=1}^{n} CCM_i \; XIM_i) + (\rho \; FLT)(FLT/2 - FLF)]/M_1 \qquad (C.4)$$

The moment of inertia was also calculated about the c.g. of the frame. Thus,

$$I_1 = \sum_{i=1}^{n} CCI_i + SIM + SIF + M_3 \; d_{20}^2 \qquad (C.5)$$

where CCI_i is the inertia value of each mass point, and

$$SIM = \sum_{i=1}^{n} CCM_i[(ZIM_i - ZCG)^2 + (XIM_i - XCG)^2]$$

$$SIF = (\rho \; FLT)[FLT^2/12 + (FLT/2 - FLF - XCG)^2 + ZCG^2].$$

APPENDIX D

DERIVATION OF THE DIGGING CHAIN FORCE

Let the tooth force (FTH) be defined as

$$FTH = FTG\ REH + VCH\ CCH\ RED \tag{D.1}$$

where

FTG = static force for the ground;

REH = reduction factor for static force;

VCH = linear chain velocity;

CCH = damping coefficient for the ground; and

RED = reduction factor for damping force.

The criteria used for determining if the teeth were cutting were the same as that described for Equation (2.36).

The total chain force was expressed as

$$RCH = FTH\ NTD \tag{D.2}$$

where NTD is the number of teeth digging. The maximum number of teeth that can dig was defined as

$$MTIG = LC/TS$$

where LC is length of chain in the ground on the digging side of the boom, and TS is the tooth spacing. The time period for one tooth is

$$TPCH = TS/VCH$$

The fraction of each tooth period of which maximum teeth are digging is

PMDG = (LC - TS MTIG)/TS

Therefore, the time of each period of which maximum teeth dig is

ATCH = PMDG TPCH

By definition

$$NTD = MTIG - 1 + XNN \tag{D.3}$$

where

XNN = 1 $\quad \tau \leq$ ATCH

XNN = 0 $\quad \tau >$ ATCH

τ represents the integration time over one complete cycle.

Equation (D.3) was substituted into Equation (D.2) which yielded

$$RCH = FTH\ (MTIG - 1 + XNN). \tag{D.4}$$

APPENDIX E

DERIVATION OF DISPLACEMENT VECTOR FOR A PLOW BLADE POINT FOR THE 3-D MODEL

The displacement of point 19 was given by Equation (3.3) as

$$\Delta_{19} = (x + \bar{d}_{19}\theta_y - b_{19}\theta_z)\ell + (y + a_{19}\theta_z - d_{19}\theta_x)m + (z + b_{19}\theta_x = \bar{a}_{19}\theta_y)n \quad \text{(E.1)}$$

The total displacement of point 21 was expressed as

$$\Delta_{21} = \Delta_{19} + \Delta_{21/19} \quad \text{(E.2)}$$

All necessary dimensions for the plow assembly are shown in Figure 2. The relative displacement of point 21 in terms of the coordinates ψ and α is

$$\Delta A_{21/19} = [-TA_2\psi - TB_1\alpha]\ell + [-TB_2\psi + TA_1\alpha]m + [TD_2\psi]n \quad \text{(E.3)}$$

where

$TA_1 = \ell_1 \cos\psi' \cos\alpha'$

$TB_1 = \ell_1 \cos\psi' \sin\alpha'$

$TA_2 = \ell_1 \sin\psi' \cos\alpha'$

$TB_2 = \ell_1 \sin\psi' \cos\alpha'$

$TD_2 = \ell_1 \cos\psi'$

Accordingly, the relative displacement in terms of coordinates θ_x and θ_y is

$$\Delta B_{21/19} = [(TA_2 \sin\alpha')\theta_x + (TB_2 \sin\alpha')\theta_y]\ell + [(-TA_2 \cos\alpha')\theta_x + (-TB_2 \cos\alpha')\theta_y]m \quad (E.4)$$

The combination of Equations (E.1) through (E.4) for the plow assembly resulted in

$$\begin{aligned}\Delta_{21} = {} & [x + (\bar{d}_{19} + TB_2 \sin\alpha')\theta_y + (TA_2 \sin\alpha')\theta_x \\ & - b_{19}\theta_z - TA_2\psi - TB_1\alpha]\ell \\ & + [y + a_{19}\theta_z - (d_{19} - TA_2 \cos\alpha')\theta_x - (TB_2 \cos\alpha')\theta_y \\ & - TB_2\psi + TA_1\alpha]m \\ & + [z + b_{19}\theta_x - \bar{a}_{19}\theta_y + TD_2\psi]n \end{aligned} \quad (E.5)$$

Points on the plow blade can only rotate in a plane, which is parallel to that of the plow boom with respect to point 21. This rotation was defined as

$$\psi_6 = CB(\psi + \theta) - \theta \quad (E.6)$$

where CB was given in Appendix A for the four-bar linkage and θ was denoted as

$$\theta = \theta_y \cos\alpha' - \theta_x \sin\alpha' \quad (E.7)$$

An axis system ℓ'''-m'''-n''' was defined where the ℓ'''-n''' plane was parallel to the boom plane and the n''' axis was directed along link ℓ_2 of the plow linkage. Thus, the position vector of any point in the plane of the plow blade was expressed as

$$\rho'''_{i/21} = \ell h_i \cos\beta \ell''' - \ell h_i \sin m''' - \ell v_i n''' \qquad (E.8)$$

where β is the angle between the blade and boom planes rotated about the n''' axis and ℓh_i and ℓv_i are the vector components of the point with respect to point 21 and measured in the blade plane. The component ℓv_i was taken along the n''' axis and ℓh_i was perpendicular to it.

The triple primed axis system was rotated an amount ψ'_1 about the m''' axis and resulted in the double primed system. Thus, Equation (E.8) was transformed into

$$\begin{aligned}\rho''_{i/21} = {} & [\ell h_i \cos\beta \cos\psi'_1 + \ell v_i \sin\psi'_1]\ell'' \\ & - [\ell h_i \sin\beta]m'' \\ & + [\ell h_i \cos\beta \sin\psi'_1 - \ell v_i \cos\psi'_1]n'' \end{aligned} \qquad (E.9)$$

The displacement of any point on the blade with respect to point 21 was caused by the rotation of ψ_6 and the rigid body rotations θ_x and θ_y. Therefore,

$$\begin{aligned}\Delta''_{i/21} = {} & -TD''_i \psi_6 \ell'' - [TD''_i \cos\alpha' \theta_x + TD''_i \sin\alpha' \theta_y]m'' \\ & + [TA''_i \psi_6 - (\ell h_i \sin\beta \cos\alpha' \theta_x + \ell h_i \sin\beta \sin\alpha' \theta_y]n'' \end{aligned} \qquad (E.10)$$

where

$$TD''_i = \ell h_i \cos\beta \sin\psi'_1 - \ell v_i \cos\psi'_1$$

$$TA''_i = \ell h_i \cos\beta \cos\psi'_1 + \ell v_i \sin\psi'_1$$

and ψ'_1 was defined for the linkage in Appendix A.

The double primed system was transformed to the unprimed system by a rotation α' about the n'' axis. Thus, Equation (E.10) was written as

$$\Delta_{i/21} = [-TD''_i \cos\alpha'\psi_6 + (TD''_i \cos\alpha' \sin\alpha')\theta_x + (TD''_i \sin^2\alpha')\theta_y]\ell$$
$$+ [-TD''_i \sin\alpha'\psi_6 - (TD''_i \cos^2\alpha')\theta_x - (TD''_i \sin\alpha' \cos\alpha')\theta_y]m$$
$$+ [TA''_i\psi_6 - (\ell h_i \sin\beta \cos\alpha')\theta_x - (\ell h_i \sin\beta \sin\alpha')\theta_y]n \quad (E.11)$$

The total displacement of any point on the plow blade was expressed as

$$\Delta_i = \Delta_{21} + \Delta_{i/21} \quad (E.12)$$

Substitution of Equations (E.5) and (E.11) into Equation (E.12) resulted in

$$\Delta_i = [x + RIY_i\theta_y - b_{19}\theta_z + RIX_i\theta_x + RIS_i\psi - TB_1\alpha]\ell$$
$$+ [y + RJZ_i\theta_z + RJX_i\theta_x + RJY_i\theta_y + RJS_i\psi + TA_1\alpha]m$$
$$+ [z + RKX_i\theta_x + RKY_i\theta_y + RKS_i\psi]n \quad (E.13)$$

where the constants are defined in terms of the system geometry and are listed in Reference (20).

APPENDIX F

MODIFICATION OF THE FRAME ASSEMBLY INERTIA PROPERTIES DUE TO THE FRONT AXLE

The frame assembly was denoted as body 1. It included the frame itself, rear axle, reel and carrier, and all other components which were rigidly attached to the frame. In the case of the digging chain, its mass and inertia were also included as part of the frame assembly. Because the front axle had only one degree of freedom, bodies 1 and 4 rotated together in two planes and separately in the other.

M_1 denoted the mass of the frame assembly and $[I_1]$ the inertia matrix. For the front axle the mass was denoted as M_4 and the inertia matrix $[I_4]$. Figures 6 and 7 show the frame and front axle. The front axle pin was connected to the frame at point 20 and allowed to rotate about a line parallel to the X-axis. Thus, the bodies were rigidly attached for motion due to the X, Z, and θ_y coordinates. The c.g. location for body 1 was defined as XCG_1, YCG_1, and ZCG_1, and the center of mass for the system was expressed as

$$\overline{XCG}_1 = (M_1\ XCG_1 + M_4 e_{20})/\bar{M}_1 \tag{F.1}$$

$$\overline{ZCG}_1 = [M_1\ ZCG_1 + M_4(g_{20} - dp_{200})]/\bar{M}_1 \tag{F.2}$$

where

$$\bar{M}_1 = M_1 + M_4.$$

Correspondingly, the inertia value for rotation in the X-Z plane about this center of mass was found to be

$$\overline{IYY}_1 = IYY_1 + M_1[(XCG_1 - \overline{XCG}_1)^2 + (ZCG_1 - \overline{ZCG}_1)^2] + IYY_4 + M_4[(\overline{XCG}_1 - e_{20})^2 + (\overline{ZCG}_1 - g_{20} + dp_{201})^2] \quad (F.3)$$

For the θ_x and y coordinates the frame and axle rotated independently but were coupled because of the pin joint. Therefore, the c.g. location in the Y-Z plane was calculated as

$$\overline{YCG}_1 = (M_1\ YCG_1 + M_4 f_{20})/\bar{M}_1 \quad (F.4)$$

The vertical height remained at ZCG_1. The inertia value for rotation about this point in the Y-Z plane was expressed as

$$\overline{IXX}_1 = IXX_1 + M_1(YCG_1 - \overline{YCG}_1)^2 + M_4(\overline{YCG}_1 - f_{20})^2 \quad (F.5)$$

For rotation in the X-Y plane the center of mass was located at (XCG_1, $\overline{YCG}_1$) and the inertia value was written as

$$\overline{IZZ}_1 = IZZ_1 + IZZ_4 + M_4(\overline{YCG}_1 - f_{20})^2 \quad (F.6)$$

After calculating the locations of the center of mass, the product of inertia terms were evaluated with Equations (F.7), (F.8), and (F.9):

$$I_{xy} = I_{x^*y^*} - m x_c y_c \quad (F.7)$$

$$I_{xz} = I_{x^*z^*} - m x_c z_c \quad (F.8)$$

$$I_{yz} = I_{y^*z^*} - m y_c z_c \quad (F.9)$$

Thus, the inertia terms were expressed as

$$\overline{IXY}_1 = IXY_1 - M_1(YCG_1 - \overline{YCG}_1)(XCG_1 - \overline{XCG}_1) - M_4(\overline{YCG}_1 - f_{20})(\overline{XCG}_1 - e_{20}) \quad (F.10)$$

$$\overline{IYZ}_1 = IXZ_1 \tag{F.11}$$

$$\overline{IYZ}_1 = IYZ_1 - M_1(YCG_1 - \overline{YCG}_1)(ZCG_1 - \overline{ZCG}_1) - M_4(\overline{YCG}_1 - f_{20})(\overline{ZCG}_1 - g_{20} + dp_{200}) \tag{F.12}$$

The modified inertia matrix $[\bar{I}_1]$ was evaluated with Equations (F.3), (F.5), (F.6), (F.10), (F.11), and (F.12).

APPENDIX G

FREQUENCY EQUATIONS FOR SINGLE DEGREE OF FREEDOM MODELS

The front axle had one degree of freedom with respect to the frame. By proper adjustment of the stiffness values for the frame assembly, this freedom was isolated. Therefore, a simple frequency equation was written. Figure 7 shows the front axle dimensions along with the generalized coordinate η.

The kinetic energy was expressed as

$$KE = \frac{1}{2} M_4 V^2 + \frac{1}{2} I_4 \omega^2 \tag{G.1}$$

where $V = dp_{200} \dot{\eta}$ and $\omega = \dot{\eta}$. The potential energy was given as

$$PE = 2[\frac{1}{2} K_3 XK_3^2 + \frac{1}{2} K_2 XK_2^2] \tag{G.2}$$

where $XK_3 = bp_{201} \eta$ $\quad XK_2 = dp_{201} \eta$. Thus, the energy expressions were written in terms of the coordinate η as

$$KE = \frac{1}{2} M_4 dp_{200}^2 \dot{\eta}^2 + \frac{1}{2} I_4 \dot{\eta}^2 \tag{G.3}$$

and

$$PE = 2[\frac{1}{2} K_3 bp_{201}^2 \eta^2 + \frac{1}{2} K_2 dp_{201}^2 \eta^2] \tag{G.4}$$

Lagrange's equation for the free vibration of a system is

$$\frac{d}{dt} (\frac{\partial KE}{\partial \dot{q}}) + \frac{\partial PE}{\partial q} = 0 \tag{G.5}$$

Equations (G.3) and (G.4) were differentiated with respect to $\dot{\eta}$ and η, respectively, and substituted into Equation (G.5) which resulted in

$$\frac{d}{dt}\left(M_4\ dp_{200}^2\ \dot{\eta} + I_4\ \dot{\eta}\right) + 2(K_3\ bp_{200}^2 + K_2\ dp_{200}^2)\eta = 0 \tag{G.6}$$

or

$$(I_4 + M_4\ dp_{200}^2)\ddot{\eta} + 2(K_3\ bp_{200}^2 + K_2\ dp_{200}^2)\eta = 0 \tag{G.7}$$

A harmonic displacement was assumed in the form of

$$\eta = \eta_o\ \sin\omega t$$

and substituted into Equation (G.7) which resulted in

$$\omega_\eta^2 = \frac{2(K_2\ dp_{200}^2 + K_3\ bp_{200}^2)}{I_4 + M_4\ dp_{200}^2} \tag{G.8}$$

For the plow assembly shown in Figure 2 the arm lengths were chosen so that the linkage was a parallelogram. Therefore, the link ℓ_2 would not rotate but only translate. The energy expressions were written as

$$KE = \frac{1}{2}\ M_2\ \ell_1^2\ \dot{\psi}^2 \tag{G.9}$$

and

$$PE = (\frac{1}{2}\ K_5 + \frac{1}{2}\ K_8)\ell_1^2\ \psi^2 \tag{G.10}$$

Substitution of these into Equation (G.5) yielded

$$M_2\ \ell_1^2\ \ddot{\psi} + \ell_1^2(K_5 + K_8)\psi = 0 \tag{G.11}$$

Thus, the frequency equation was expressed as

$$\omega_\psi^2 = \frac{K_5 + K_8}{M_4} \tag{G.12}$$

Figure 5 shows the plow assembly with the α degree of freedom. The value of α' was set to zero. Thus, the boom rotated about point 30 with the restoring force created by spring elements K_{30} and K_{15}. Again the energy functions were written as

$$KE = \frac{1}{2} M_2 a^2 \dot{\alpha}^2 + \frac{1}{2} IZZ_2 \dot{\alpha}^2 \tag{G.13}$$

and

$$PE = \frac{1}{2} K_{15} d^2 \alpha^2 + \frac{1}{2} K_{30} \alpha^2 \tag{G.14}$$

where $a = e_{22} - e_{19}$ and $d = e_6 - e_{19}$. The combination of Equations (G.5), (G.13), and (G.14) resulted in

$$(IZZ_2 + M_2 a^2)\ddot{\alpha} + (K_{15} d^2 + K_{30})\alpha = 0 \tag{G.15}$$

Correspondingly, the frequency equation was obtained as

$$\omega_\alpha^2 = \frac{K_{15} d^2 + K_{30}}{IZZ_2 + M_2 a^2} . \tag{G.16}$$

VITA

David Lynn Turney

Candidate for the Degree of

Doctor of Philosophy

Thesis: A DEVELOPMENT OF A DYNAMIC ANALYSIS TECHNIQUE FOR VEHICLE FRAMES OF VIBRATORY PLOW AND TRENCHERS

Major Field: Mechanical Engineering

Biographical:

Personal Data: Born February 18, 1951, in Heber Springs, Arkansas, the son of Mr. and Mrs. R. L. Turney.

Education: Graduated from Quitman High School, Quitman, Arkansas, in May, 1969; received the Bachelor of Science degree in Mechanical Engineering in 1973 from Louisiana Tech University; received the Master of Science degree in 1975 from Oklahoma State University; completed the requirements for the Doctor of Philosophy degree at Oklahoma State University in July, 1978.

Professional Experience: Graduate Teaching Assistant, Oklahoma State University, 1973-1975; Graduate Research Assistant, Oklahoma State University, 1975-1978.

Professional Organizations: Tau Beta Pi, Pi Tau Sigma, Phi Kappa Phi.